TRIBHUVAN UNIVERSITY

# INSTITUTE OF ENGINEERING

## PULCHOWK CAMPUS

**THESIS NO: 079/MSPDE/013**

**A THESIS REPORT ON**

# Performance Enhancement with CFFNN and GA in MPPT Techniques and Implementation of ANFIS Controllers to Improve the Power Quality of Grid Connected PV System with Cascaded Multilevel Inverter


**BY**

**MADHUSUDAN NYAUPANE**

**(079/MSPDE/013)**


**A THESIS SUBMITTED TO**

**MASTER OF SCIENCE IN POWER ELECTRONICS AND DRIVES ENGINEERING**

**DEPARTMENT OF ELECTRICAL ENGINEERING, LALITPUR, NEPAL**

**APRIL, 2025**

# Performance Enhancement with CFFNN and GA in MPPT Techniques and Implementation of ANFIS Controllers to Improve the Power Quality of Grid Connected PV System with Cascaded Multilevel Inverter

**By**

**Madhusudan Nyaupane**

**(079/MSPDE/013)**

**Thesis Supervisor**

**Associate Prof. Jeetendra Chaudhary**

**A thesis submitted in partial fulfillment of the requirements for the degree of Master of Science in Power Electronics and Drives Engineering**

Department of Electrical Engineering Institute of Engineering, Pulchowk Campus Tribhuvan University

Lalitpur, Nepal

April, 2025

# COPYRIGHT ©

त्रिभुवन विश्वविद्यालय
TRIBHUVAN UNIVERSITY
इन्जिनियरिङ्ग अध्ययन संस्थान
INSTITUTE OF ENGINEERING
पुल्चोक क्याम्पस
PULCHOWK CAMPUS
DEPARTMENT OF ELECTRICAL ENGINEERING
Pulchowk, Lalitpur

Accredited by University Grants Commission (UGC) Nepal 2020



## CERTIFICATE OF APPROVAL

The undersigned certify that they have read and recommended to the Institute of Engineering for acceptance, a thesis entitled "**Performance Enhancement with CFFNN and GA in MPPT Techniques and Implementation of ANFIS Controllers to Improve the Power Quality of Grid Connected PV System with Cascaded Multilevel Inverter**", submitted by **Madhusudan Nyaupane** in partial fulfillment of the requirement for the degree of **Master of Science in Power Electronics and Drives Engineering.**

Assoc. Prof. Jeetendra Chaudhary
Department of Electrical Engineering
Pulchowk Campus, Lalitpur
(Supervisor)

Asst. Prof. Dr. Rajesh M. Pindoriya
Thapar Institute of Engineering and Technology, Punjab, India
(Supervisor)

Dr. Laxman Maharjan
Former Assistant Manager
Corporate R&D Headquarters, Fuji Electric Co., Ltd., Japan
(External Examiner)

Assoc. Prof. Jeetendra Chaudhary
Program Coordinator
M. Sc. Power Electronics and Drives Engineering
Pulchowk Campus, Lalitpur

Assoc. Prof. Dr. Basanta K. Gautam
Head of Department
Department of Electrical Engineering
Pulchowk Campus, Lalitpur

April 2025



Tel: +977-1-5443081, Email: doee@pcampus.edu.np, Website: www.doee.pcampus.edu.np

# ACKNOWLEGEMENT

I would like to express my deep sense of gratitude to my supervisor Jeetendra Chaudhary, Program Co-ordinator, Master of Science in Power Electronics and Drives Engineering, for his valuable guidance, co-operation with useful suggestions that really helped me to carry out my thesis work. I extend my sincere gratitude to Yubraj Adhikari, Head, Department of Electrical Engineering, for providing opportunity to carry out thesis work on " Performance Enhancement with CFNN and GA in MPPT Techniques and Implementation of ANFIS Controllers to Improve the Power Quality of Grid Connected PV System with Cascaded Multilevel Inverter " as one of the requirements for the master's degree.

It my pleasure to express my deep sense of gratitude to Prof. Dr. Navaraj Karki, Associate Prof. Dr. Basanta Kumar Gautam as well as all the faculties of Department of Electrical Engineering, Institute of Engineering, Pulchowk Campus for their valuable comments, suggestions and direction of this thesis work.

I would like to express special thanks to Prof. Dr. Prof. Sukumar Mishra, Assistant Prof. Dr. Soumyabrata Barik and Assistant Prof. Dr. Vedantham Lakshmi Srinivas for providing their valuable suggestions and ideas during simulation work of AI based nine level Inverter for improvement of power quality issues in grid connected system.

I extend my sincere appreciation to the Indian Institute of Technology, Indian School of Mines, Dhanbad for providing the necessary resources and facilities for this research. I would like to express my heartfelt thanks to my family and friends for continuous support and help.

Finally, I would like to acknowledge all the authors and researchers whose work has contributed to my understanding of power quality issues and their mitigations in grid connected inverter system and in active distribution networks due to integration of inverter-based resources in a microgrid.

# ABSTRACT

This thesis presents an efficient and robust GA-based MPPT algorithm for photovoltaic (PV) systems, designed to enhance power output stability and tracking speed. The proposed approach minimizes power oscillations at the Maximum Power Point (MPP) and improves conventional MPPT methods through global optimization, making it ideal for dynamic environmental conditions. Furthermore, a Machine Learning (ML)-based three-phase nine-level Pulse Width Modulation (PWM) inverter has been developed and simulated for grid-connected PV applications. The inverter is controlled using an Adaptive Neuro-Fuzzy Inference System (ANFIS)-based current controller, ensuring precise modulation and grid synchronization. Furthermore, a Cascaded Feedforward Neural Network (CFFNN)-based MPPT algorithm is employed for maximum power extraction. A boost converter is used to regulate the DC-link voltage, dynamically adjusting its duty cycle based on the MPPT strategy. The system is designed for seamless integration with a three-phase utility grid, efficiently managing both linear and nonlinear loads. The output voltage and frequency are precisely regulated to maintain a unity power factor (UPF), ensuring optimized energy transfer. The ANFIS-based current control maintains sinusoidal grid current and provides a fast dynamic response under fluctuating irradiance and temperature conditions. The Total Harmonic Distortion (THD) is analyzed using Fast Fourier Transform (FFT) techniques, verifying compliance with IEEE 519 standards and demonstrating high power quality. The system's performance is validated through MATLAB/Simulink simulations, with results aligning closely with theoretical expectations, proving its effectiveness in MPPT enhancement, inverter efficiency, and grid stability. These findings indicate that the proposed system is well-suited for experimental implementation, offering valuable contributions to the integration of renewable energy into modern power grids.

***Keywords: Cascaded Feed Forward Neural Network (CFFNN), Adaptive Neuro Fuzzy Interface System (ANFIS) Controller, Cascaded Multilevel Inverter (CMLI), Genetic Algorithm (GA), Total Harmonic Distortion (THD), Power Quality (PQ).***

# TABLE OF CONTENTS

**Content** **Page**

# LIST OF FIGURES

**Content** **Page**

# LIST OF TABLES

**Content** **Page**

# LIST OF SYMBOLS

| | |
|---|---|
| ω | Angular Frequency |
| KV | Kilovolts |
| π | Pi |
| KW | Kilowatts |
| A | Amperes |
| $\mu$s | Micro-second |
| $n$s | Nano second |
| $\mu$ | Adaptive Learning Rate |

# ACRONYMS

| | |
|---|---|
| CFFNN | Cascaded Feed Forward Neural Network |
| MPPT | Maximum Power Point Tracking |
| PV | Photovoltaic |
| ML | Machine Learning |
| ANFIS | Adaptive Neuro Fuzzy Interface System |
| CMLI | Cascaded Multilevel Inverter |
| GA | Genetic Algorithm |
| THD | Total Harmonic Distortion |
| PQ | Power Quality |
| FFT | Fast Fourier Transform |
| UPF | Unity Power Factor |
| PWM | Pulse Width Modulation |
| GCI | Grid Connected Inverter |
| RES | Renewable Energy Source |
| EMI | Electromagnetic Interference |
| DG | Distributed Generation |
| IBR | Inverter Based Resources |
| DER | Distributed Energy Resources |
| BESS | Battery Energy Storage System |
| EV | Electric Vehicles |

| | |
|---|---|
| VFD | Variable Frequency Drives |
| LED | Light Emitting Diodes |
| UPS | Uninterruptible Power Supply |
| AND | Active Distribution Network |
| D- STATCOM | Distribution Static Compensator |
| UPQC | Unified Power Quality Conditioner |
| TVSS | Transient Voltage Surge Suppressors |
| DVR | Dynamic Voltage Restorer |
| PI | Proportional-Integral |
| PLC | Programmable Logic Controller |
| P & O | Perturb and Observe |
| INC | Incremental Conductance |
| CCM | Continuous Conduction Mode |
| DC | Direct Current |
| AC | Alternating Current |
| GCI | Grid Connected Inverter |
| FLC | Fuzzy Logic Controller |
| PCC | Point of Common Coupling |
| NL | Negative Large |
| NM | Negative Medium |
| NS | Negative Small |
| PS | Positive Small |

| | |
|---|---|
| PM | Positive Medium |
| PL | Positive Large |
| Z | Zero |
| CSI | Voltage Source Inverter |
| VSI | Current Source Inverter |
| ISCT | Instantaneous Symmetrical Component Theory |
| RMS | Root Mean Square |
| ANN | Artificial Neural Network |
| HC | Hill Climbing |
| ABC | Artificial Bee Colony |
| PSO | Particle Swarm Optimization |
| MMC | Modular Multilevel Cascaded |
| ICA | Imperialist Competitive Algorithm |
| IMMLI | Integrated Module Multilevel Inverter |
| TSV | Total Stress Voltage |
| MVS | Maximum Voltage Stress |
| MOSFET | Metal Oxide Semiconductor Field Effect Transistor |
| RLU | Rectified Linear Unit |
| CMLI | Cascaded Multilevel Inverter |
| PLL | Phase Locked Loop |
| SPWM | Sinusoidal Pulse Width Modulation |

| | |
|---|---|
| MFs | Membership Functions |
| DFT | Discrete Fourier Transform |
| MATLAB | MATrix LABoratory |
| DS | Distribution System |
| VSC | Voltage Source Converter |
| SLD | Single Line Diagram |
| DSP | Digital Signal Processing |
| SCR | Short Circuit Ratio |
| FRT | Fault Ride Through |
| FPGA | Field Programmable Gate Array |
| NPC | Neutral Point Clamp |

# 1. INTRODUCTION

## 1.1 Background and Motivation

Conventional fossil fuels such as petroleum, natural gas, and coal primarily supply the world's energy needs. However, their availability is gradually declining, and the byproducts they produce contribute significantly to environmental issues like the greenhouse effect [1]. Renewable Energy Sources (RES), including wind, tidal, solar, geothermal, and biomass, have become key areas of research and development. Among these, photovoltaic (PV) technology is widely adopted due to advancements in fabrication techniques, making PV devices more affordable and accessible [2]. The PV generator transforms solar energy into electrical energy and offers several advantages, including being pollution-free, having no moving parts, minimizing wear and tear, being freely available and abundant, and having a long lifespan of over 20 years [3]. A significant advancement in power electronics is the development of Multilevel Inverters (MLIs). These inverters facilitate efficient power conversion while improving power quality by reducing Total Harmonic Distortion (THD) and Electromagnetic Interference (EMI), as well as requiring smaller filter sizes [4]. As a result, MLIs have gained popularity and demand due to their advantages over conventional inverters. Additionally, they can handle higher power and voltage levels while reducing voltage stress on power electronic switches [5]. However, the presence of power electronic converters, nonlinear loads, and distributed generation (DG) introduces harmonics, leading to power quality issues such as voltage distortion, overheating, and reduced efficiency of electrical equipment. The integration of renewable energy sources and energy storage systems, along with the rising electricity demand, high costs of large power plants, and environmental concerns, has highlighted the need for innovative planning, operation, and control strategies in power distribution networks [6]. Power quality may be defined as “the measure, analysis, and improvement of bus voltage, usually a load bus voltage, to maintain that voltage to be a sinusoid at rated voltage and frequency” [7]. The various sources of harmonics in grid connected Photovoltaic ( PV) system are primarily caused by the following: Power Electronic Converters; DC-AC inverters, rectifiers, and DC-DC converters used in energy storage systems and IBRs contribute to harmonic distortion, Distributed Energy Resources (DERs):

Solar PV Inverters generate harmonics due to pulse-width modulation (PWM) switching, Wind Energy Converters with power electronic interfaces introduce harmonics due to the variable nature of wind power, Battery Energy Storage Systems (BESS) use bidirectional converters, which inject harmonic components; Nonlinear Loads: Electric vehicle (EV) chargers and fast-charging stations draw non-sinusoidal current, leading to harmonic distortion, Variable Frequency Drives (VFDs) used in industrial loads introduce significant harmonic currents, LED lighting and UPS systems also contribute to harmonics in the low-voltage distribution network, Unbalanced and Fluctuating Loads: Unequal phase loading in three-phase systems leads to the presence of triplen harmonics (3rd, 9th, 15th harmonics), Rapid load fluctuations in grid connected system cause transient harmonics, affecting voltage stability. Power quality issues in power systems can be classified into several categories. These are voltage unbalance, voltage flicker, voltage sags and swells, interruptions, and voltage and current harmonics [8]. The harmonics phenomenon is a prominent issue of power quality. Harmonics are unwanted frequency components in electrical systems that are integer multiples of the fundamental frequency (e.g., 50 Hz). In modern Active Distribution Networks (ADNs) with renewable energy sources, electric vehicle (EV) charging stations, and power electronic converters, harmonic distortion is a critical power quality issue that needs to be analyzed and mitigated. [9] discusses the power quality issues for distributed generation systems based on renewable energy sources, such as solar and wind energy. In [9], power quality monitoring techniques and possible solutions of the power quality issues for the power systems are elaborately studied and then analyses the methods of mitigation of these problems using custom power devices, such as D-STATCOM, UPQC, UPS, TVSS, DVR, etc., for micro grid systems. According to [10], the various types of power quality problems along with their effects are as represented in table 1.1.

*Table 1.1: PQ issues, causes, effects and severity*

| **Power Quality Issues** | **Causes** | **Effects** | **Severity** |
|---|---|---|---|
| Voltage Drop | High inrush current, large load start-up, switching operations, inadequate wiring | Loss of system performance, equipment malfunctions, data errors | Severe |
| Voltage Sag | Sudden load increase, equipment faults, short circuits, starting of heavy motors | Equipment failure, reduced efficiency, disruption of operations | moderate |
| Voltage Swell | Sudden decrease in load, faulty regulator operation, equipment disconnection | Overheating of components, potential for equipment damage | moderate |
| Long-Term Voltage Disruption | Sustained supply failures, control system issues, unstable voltage levels | Prolonged equipment downtime, production interruptions | Severe |
| Noise | Electromagnetic interference, poor grounding practices | Performance disruption in electronic devices | Mild |
| Waveform Distortion | Presence of noise in supply systems | Overloading, inefficiency, and equipment malfunction | Severe |
| Frequency Variations | Heavy load fluctuations, grid instability | Impact on motors and sensitive electrical equipment | Mild |
| Harmonics | Non-linear loads, power electronics, distorted waveforms | Losses in transformers, overheating, reduced equipment lifespan | moderate |
| Voltage Spikes | Switching heavy loads, power surges, faulty power regulation | Data corruption, equipment failure, component burnout | Severe |
| Transients | Lightning strikes, switching surges, sudden load changes | Damage to electronic circuits and components | Catastrophic |

| | | | |
|---|---|---|---|
| Flicker | Rapid load changes, inadequate supply voltage control | Discomfort to users, disruption to lighting equipment | moderate |
| Spinning Reserve | Insufficient backup generation, load fluctuations | Voltage instability, failure to meet power demand | Mild |

As discussed in table 1.1, these PQ issues must be mitigated to enhance the reliability of loads and to maintain the continuity of supply. The global transition to renewable energy has highlighted the importance of maintaining power quality in distribution grids. IEEE 519 Standard gives a proper guideline for harmonics analysis. For harmonics voltage table 1.2 is applicable and for harmonic currents with integer multiples of the power frequency, table 1.3 is applicable [11].

*Table 1.2: Voltage distortion limits*

| **Bus Voltage V** | **Individual harmonic (%)** | **THD (%)** |
|---|---|---|
| V ≤ 1.0 KV | 5.0 | 8.0 |
| 1.0 KV ≤ V≤ 69 KV | 3.0 | 5.0 |
| 69 KV ≤ V ≤ 161 KV | 1.5 | 2.5 |
| 161 KV < V | 1.0 | 1.5 |

*Table 1.3: Current Distortion Limits*

| Maximum harmonic current distortion in percent of IL | | | | | | |
|---|---|---|---|---|---|---|
| Individual harmonic order (odd harmonics) | | | | | | |
| ISC/IL | 3 ≤ h ≤ 11 | 11 ≤ h ≤ 17 | 17 ≤ h ≤ 23 | 23 ≤ h ≤ 35 | 35 ≤ h ≤ 50 | TDD |
| <20 | 4.0 | 2.0 | 1.5 | 0.6 | 0.3 | 5.0 |
| 20<50 | 7.0 | 3.5 | 2.5 | 1.0 | 0.5 | 8.0 |
| 50<100 | 10.0 | 4.5 | 4.0 | 1.5 | 0.7 | 12.0 |
| 100<1000 | 12.0 | 5.5 | 5.0 | 2.0 | 1.0 | 15.0 |
| >1000 | 15.0 | 7.0 | 6.0 | 2.5 | 1.4 | 20.0 |

Firstly, different MPPT techniques P & O, Incremental Conductance and Genetic Algorithm based MPPTs are analyzed and compared. After that CFFNN based MPPT is designed to omit the problem of power oscillations in the output of boost converter. Based on these IEEE 519 Standard, THDs in any grid connected system are observed and ANFIS based multilevel inverters are designed and optimized

along with the CFFNN based MPPT system to improve the power quality issues in a distribution micro grid.

## 1.2 Problem Statement

Currently grid connected PI controller-based inverters are being used and P & O, Incremental Conductance MPPT algorithms are implemented with the PV system but when MPPT is reached, Perturb and observe (P and O) algorithm will oscillate around maximum power point (MPP) and will search in the wrong direction by considering only power variations. Unlike P and O, Incremental Conductance will resolve the problem of power variation based on change in power with respect to change in voltage $\left(\frac{dp}{dv}\right)$ but there is the slow convergence in the maximum power and problem with the partial shading conditions. Grid-connected photovoltaic (PV) systems have gained widespread adoption due to their ability to generate clean and renewable energy. However, integrating PV systems with the grid introduces several power quality challenges that can affect both the system's performance and the stability of the electrical network. These issues primarily include voltage sag, voltage swell, harmonic distortion, and waveform distortions. Power quality issues in grid-connected PV systems can significantly impact both the performance of the PV system and the stability of the power grid. The main causes of the harmonic distortions in the grid connected PVs system are Pulse Width Modulation (PWM) switching of power electronic inverters. Interaction of inverters with the grid impedance. Poorly designed inverter filters. Due to THDs in the grid connected PVs system cause the following impacts:

- Increased losses in power transformers and cables.
- Overheating of motors and generators.
- Malfunctioning of sensitive electronic devices and relays.
- Harmonics can distort the voltage waveform, causing flickering lights and unstable voltage levels. This can lead to discomfort for users and impact precision equipment in industries.
- Certain harmonics can interact with system capacitances and inductances, leading to resonant conditions. This can amplify voltage and current distortions, causing severe damage to components.

- Harmonics cause increased dielectric stress and heating in capacitors used for power factor correction. This leads to premature capacitor failure and increased maintenance costs.
- Meters, sensors, and power analysers may provide incorrect readings due to harmonic interference. This affects energy billing, monitoring, and control systems.
- High-frequency harmonics can interfere with data transmission and communication lines in smart grids and industrial automation systems. This results in data corruption, signal distortion, and reduced efficiency of PLCs (Programmable Logic Controllers).

To minimize these effects and maintain power quality, several mitigation techniques are used, including active harmonic filters, multilevel inverters (MLIs), and improved grounding methods. One step solution is the use of ML based Multilevel Inverters (MLIs). Multilevel Inverters (MLIs) are advanced power converters that generate near-sinusoidal voltage waveforms using multiple voltage levels. This reduces Total Harmonic Distortion (THD) and enhances power quality. Instead of a single two-level switching operation, MLIs produce a staircase-like waveform that closely resembles a pure sine wave. This minimizes high-frequency harmonic components, reducing the need for extensive filtering. The higher the number of levels, the lower the harmonic distortion in the output waveform.

## 1.3 Objective

The main objective of this thesis is to analyze and improve the power quality issues with the grid connected PV system using the ANFIS based inverter and CFFNN based MPPT techniques. But the specific objectives are as follows.

i. To design and compare the different MPPT algorithms: P& O, Incremental Conductance Genetic Algorithm
ii. Development of CFFNN (Machine Learning) based MPPT algorithm.
iii. To design and optimize the ANFIS based grid connected inverter.
iv. To analyze the THDs using Fast Fourier Transform (FFT) technique.

## 1.4 Scope of Thesis

This thesis focuses on enhancing power quality in grid-connected PV systems by integrating advanced control techniques, specifically ANFIS-based inverters and Cascaded Feedforward Neural Network (CFFNN)-based MPPT algorithms. The study aims to address power quality issues such as harmonic distortion, voltage fluctuations, and efficiency improvements. The scope of this research includes the following aspects:

- Evaluation of traditional and advanced MPPT algorithms, including Perturb & Observe (P&O), Incremental Conductance, and Genetic Algorithm-based MPPT and CFFNN ML based algorithm and identification of the most efficient algorithm in terms of tracking speed, steady-state oscillations, and energy harvesting efficiency.
- Development of an Adaptive Neuro-Fuzzy Inference System (ANFIS) based inverter for grid integration and optimization of switching strategies and control parameters to minimize Total Harmonic Distortion (THD) and improve power factor correction.
- Analysis of Total Harmonic Distortion (THD) using the Fast Fourier Transform (FFT) technique, evaluation of harmonic mitigation strategies to ensure compliance with IEEE 519 harmonic standards and performance assessment of the ANFIS inverter in reducing harmonic content and improving voltage waveform quality.
- Enhancement of power stability and efficiency in grid-connected PV systems, contribution to the advancement of intelligent control methods for renewable energy systems and potential implementation of the proposed approach in smart grids and distributed generation networks.

## 1.5 Publications

Research papers related to performance and enhancement of MPPT Techniques using Genetic algorithm is published in the journal listed below.

- M. Nyaupane, S. Adhikari, G. Gupta and S. Tiwari, "Comparison and Performance Enhancement of Maximum Power Point Tracking Technique for Photovoltaic Systems using Genetic Algorithm," *2024 IEEE International Conference on Power System Technology (PowerCon)*, Kathmandu, Nepal, 2024, pp. 1-5, doi: 10.1109/PowerCon60995.2024.10870561.

The paper under review is listed below.

- Optimal Energy Management in Hybrid Energy Storage System for Power Transients- Electric Power Systems Research, Elsevier

## 1.6 Thesis Outline

The outline of remaining portion of the thesis is arranged as follows,

In chapter 2 Literature survey regarding the MPPT techniques and Multilevel inverters and control techniques along with the identified research gap are discussed. Chapter 3 presents the research methodology discussed on three steps to carry out the whole thesis work as CFFNN MPPT and GA based techniques for PV output, ANFIS Based CMLI and their control techniques to improve the harmonics in output voltage and Current and THD analysis in GCI. Simulation diagrams and results of Cascaded 9 level GCI with CFFNN MPPT and ANFIS based current regulator along with the LCL filter for power quality improvement in 19 bus system are presented in chapter 4, where different MPPT techniques along with ML based MPPT and ML based GC 9 level inverter with THD analysis is discussed in detail.

The THD values in different load buses, load voltage and current's THDs and comparison with the IEEE 519 standard and ML based multilevel inverter and ML based MPPT with PQ improvement are summarized as conclusion of the thesis in chapter 5 and some postulates for future enhancement are also mentioned that validation through experimental setup and implement fault ride-through (FRT) capability to ensure compliance with modern grid codes.

# 2. LITERATURE REVIEW

## 2.1 Conventional Maximum Power Point Techniques

### 2.1.1 Perturb and Observe MPPT method

The Perturb & Observe (P&O) algorithm is a widely adopted conventional method for tracking the Maximum Power Point (MPP) in commercial PV controllers, primarily due to its simplicity The Perturb and Observe (P&O) algorithm operates by introducing a small perturbation in the voltage and monitoring the corresponding change in power output. If increasing the voltage results in a power increase, the system is operating on the left side of the MPP; conversely, if the power decreases, it indicates operation on the right side of the MPP. In summary, this process is effectively demonstrated in Table 2.1 [13]. The P&O algorithm flowchart is demonstrated in Fig. 2.2.

*Table 2.1: P & O Algorithm Summary*

| Voltage Adjustment | Power Response | Next Voltage Adjustment |
|---|---|---|
| Increase | Increases | Continue Increasing |
| Increase | Decreases | Start Decreasing |
| Decreases | Increases | Continue Decreasing |
| Decreases | Decreases | Start Increasing |

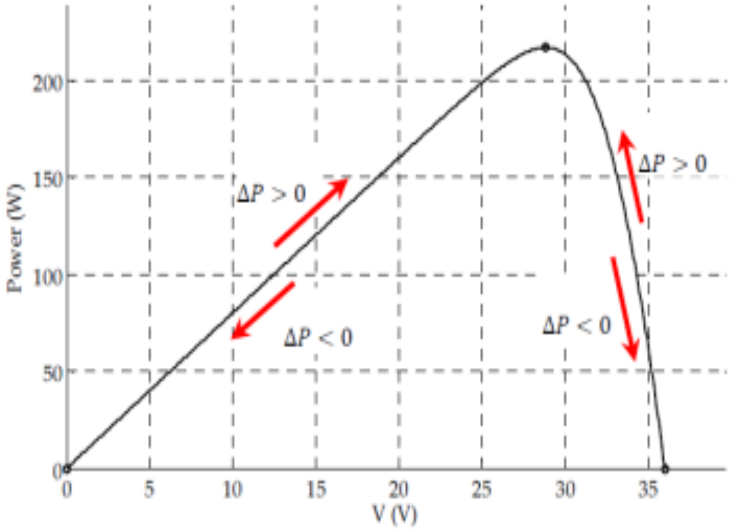


Fig. 2.1. Conventional PO Method

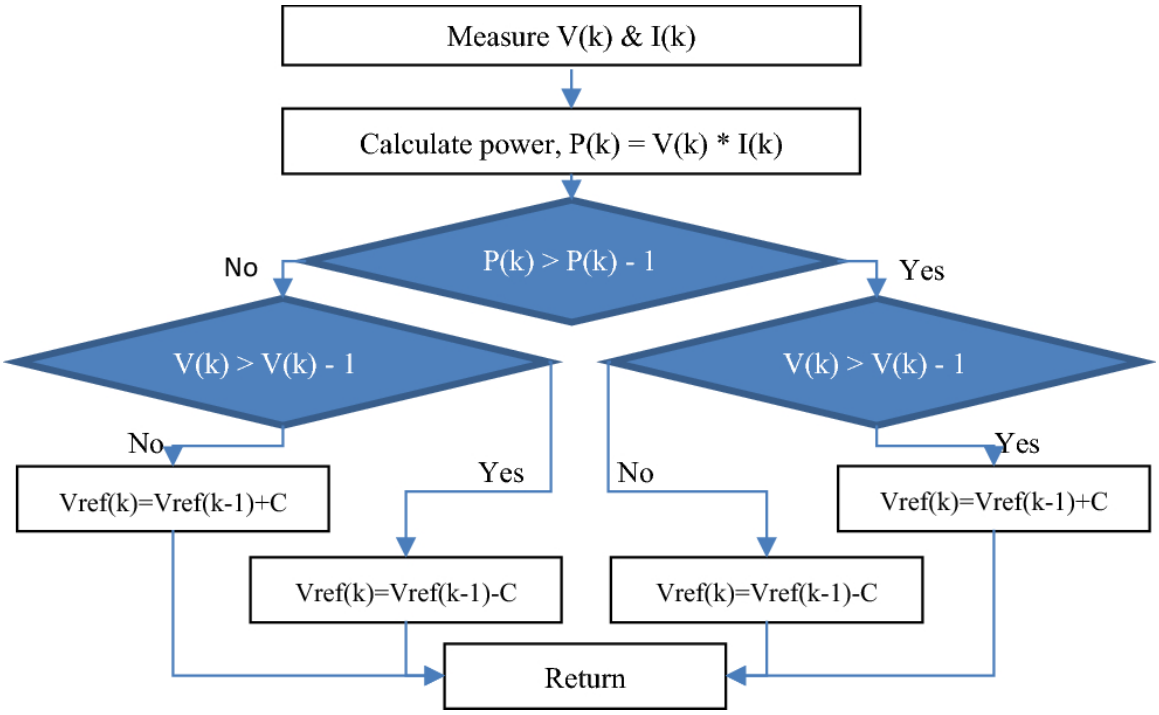


Fig. 2.2. Flowchart of P&O MPPT technique [14]

Where, V(k) represents the current PV output voltage, while V(k−1) denotes the previous PV output voltage. Similarly, I(k) refer to the current PV output current, and P(k) is the current PV output power, whereas P(k−1) represents the previous PV output power. Additionally, $V_{ref}$ is the reference output voltage determined by the P&O controller.

However, it has two significant limitations. Firstly, it exhibits persistent oscillations around the MPP, leading to continuous fluctuations in output power. As a result, energy losses occur, ultimately reducing the overall efficiency of the PV system. Secondly, the P&O algorithm struggles with rapid changes in weather conditions. During sudden variations in solar irradiance or temperature, it may deviate from the MPP and fail to track it accurately, causing further energy losses and affecting system performance [12].

### 2.1.2 Incremental Conductance MPPT method

The Incremental Conductance (INC) method operates on the principle that power reaches its maximum point when its differential with respect to voltage equals zero. On the P-V characteristic curve, the rate of change of power with respect to voltage can be zero, positive, or negative, depending on the position relative to the

Maximum Power Point (MPP). Specifically, this differential is zero at MPP, positive on the left of MPP, and negative on the right of MPP. The operational principle of this method is outlined as follows:

$$\frac{dP}{dV} = \frac{d(I.V)}{dV} = V.\frac{dI}{dV} + I \quad (2.1)$$

So, at MPP we can write:

$$\frac{dP}{dV} = 0 => \frac{dI}{dV} = -\frac{I}{V} \quad (2.2)$$

It can be observed that the MPP is determined by comparing the incremental and instantaneous conductance, where:

$$\frac{dI}{dV} > -\frac{I}{V} \rightarrow \text{Increase PV array voltage (V)} \quad (2.3)$$

$$\frac{dI}{dV} < -\frac{I}{V} \rightarrow \text{Ddecrease PV array voltage (V)} \quad (2.4)$$

$$\frac{dI}{dV} \sim -\frac{I}{V} \rightarrow \text{At the MPP} \quad (2.5)$$

The Incremental Conductance method can be illustrated graphically in the following figure 2.3.

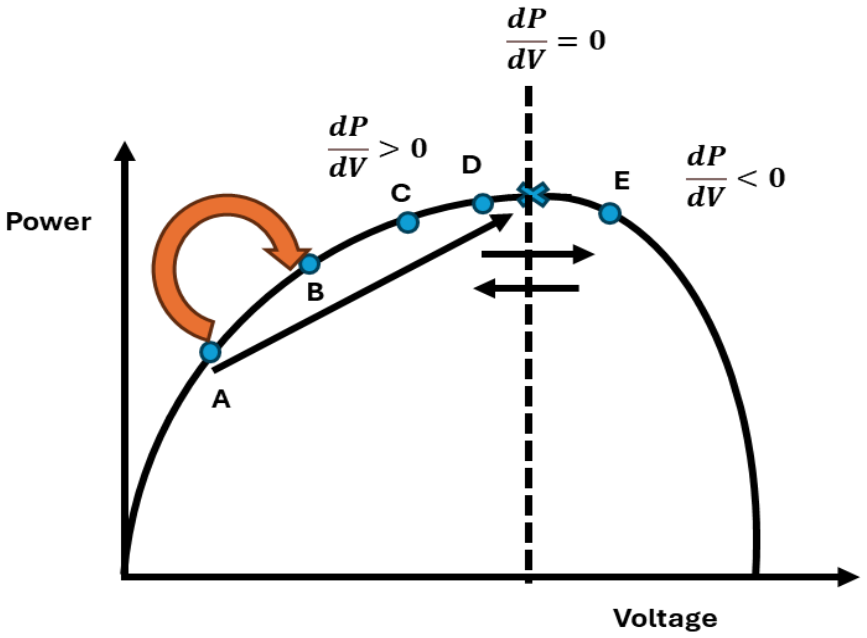


Fig. 2.3. Conventional INC method

This method offers reduced oscillations around the MPP, resulting in stable operation. However, its primary drawback is its higher complexity compared to the Perturb and Observe (P&O) method.

The flowchart of INC method algorithm is as shown in figure 2.4.

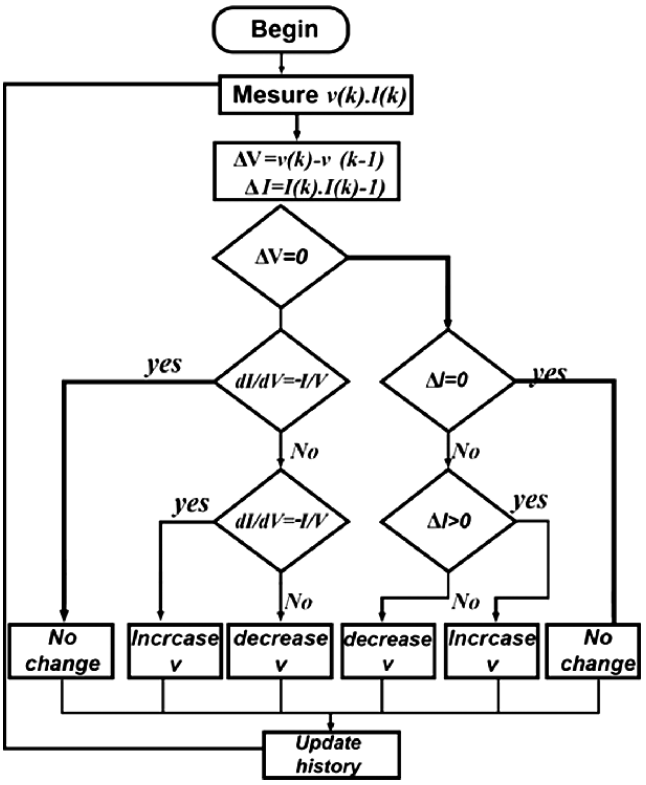


Fig. 2.4. Flowchart of INC Algorithm [15]

Genetic algorithm is used to design and simulate the model for keeping the system operating point at Maximum Power Point (MPP) so it guarantees that the search process starts from the closest point to the MPP and try to reach the target point in the shortest time. This study's novelty lies in its focus on the Genetic Algorithm for MPPT, addressing the dispersed and critically unexamined information in existing research, thereby offering a valuable foundation for future researchers and aiding the solar industry in developing innovative MPPT controllers with improved tracking capabilities.

## 2.2 Boost Converter for PV MPPT

The DC-DC step-up converter operates in two modes. The basic difference in both the modes is the flow of inductor current. In the first mode, the current through the inductor flows continuously, whereas in the second mode, the current through the inductor comes to zero for an interval of time before the next turn-on of the switch Again, the CCM mode operates in two ways, i.e., turn on mode (Mode 1) and turn off mode (Mode 2). During Mode 1, the power switch is turned ON. As a result, when the switch is turned ON, the supply current input to the circuit follows a path through the inductor connected in series with the power switch. In this mode, the energy is stored in the inductor, while the capacitor supplies the load. Mode 2

operation starts when the power switch is turned OFF. In this mode, as the switch is OFF, no more current flows through this path, and instead, the current flows through the inductor, diode, capacitor, and resistive load. Figure 4 shows the path of current flow during the turn-off process. During this period, the stored energy in the inductor is discharged to the resistive load. Thus, the terminal voltage is higher than the supply voltage, which is why it is called a step-up or boost converter. In the CCM mode, the current through the inductor never reaches zero. The value of inductance and capacitance calculation methods are described in [40]. The value of inductance can be calculated using the equation:

$$\boldsymbol{L}_{\min} = \frac{(\mathbf{1}-\boldsymbol{D})^{\mathbf{2}}\times \boldsymbol{D}\times \boldsymbol{R_0}}{\mathbf{2}\times \boldsymbol{F_s}} \tag{2.6}$$

Where, $\boldsymbol{D}$ = duty cycle of boost converter, which is given by,

$$\boldsymbol{D} = \mathbf{1} - \frac{\boldsymbol{V_{in}}}{\boldsymbol{V_o}} \tag{2.7}$$

$\boldsymbol{F_s}$= switching frequency

$\boldsymbol{R_0}$= load resistance

And the minimum capacitance value $\boldsymbol{C}_{\min}$ is given by:

$$\boldsymbol{C}_{min} = \frac{\boldsymbol{D}}{\boldsymbol{R_0}\times \boldsymbol{V_{rf}}\times \boldsymbol{F_s}} \tag{2.8}$$

The voltage ripple factor $\boldsymbol{V_{rf}}$ is given by:

$$\boldsymbol{V_{rf}} = \frac{\boldsymbol{\Delta V_o}}{\boldsymbol{V_o}} \tag{2.9}$$

## 2.3 PI-Based Controller with Grid Connected Inverter

The PI controller is used with the grid connected inverter to calculate the current regulator gain provided in figure 2.5 and 2.6. A PI Controller is a type of control system widely used in industrial applications, including power electronics, motor drives, and renewable energy systems. It is a combination of Proportional (P) and Integral (I) control actions, providing both fast response and zero steady-state error [18].

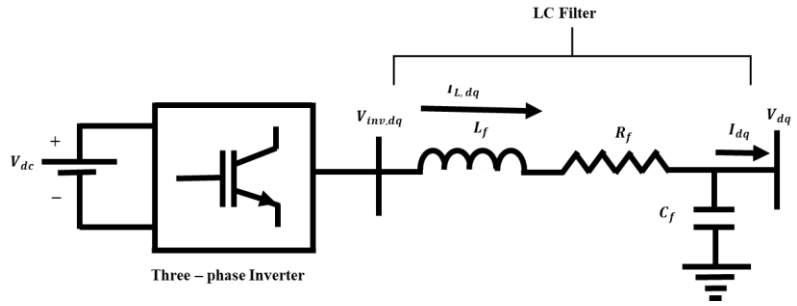


Fig. 2.5. Three Phase Grid Connected Inverter [18]

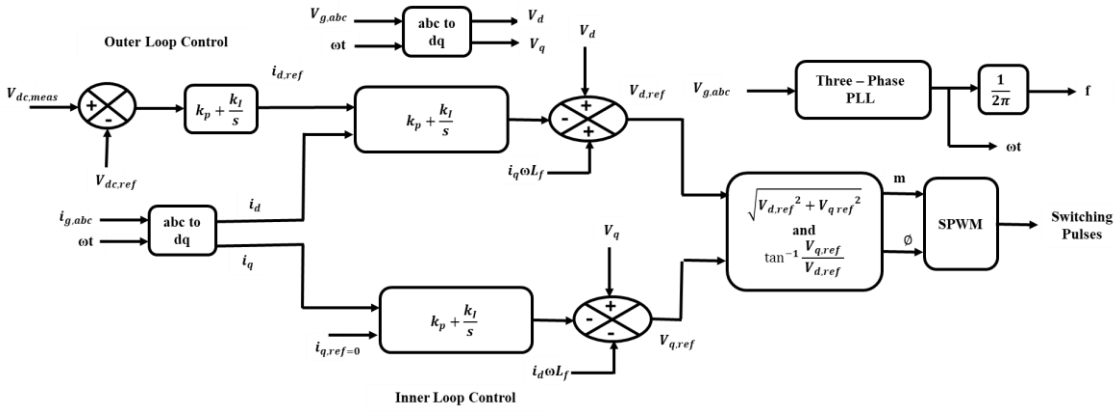


Fig. 2.6. Three Phase Grid Connected Inverter with PI Controllers [19]

The transfer function of an ideal PI controller is defined as,

$$G_f(s) = K_p + \frac{K_i}{s} = \frac{K_p s + K_i}{s} = K_i\left(1 + \frac{1}{T_i s}\right) \quad (2.10)$$

If a first-order low-pass filter with a cut-off frequency $\omega_c$ is used in the synchronous frame, the transfer function of the ideal PI controller becomes,

$$G_f(s) = K_p + \frac{K_i \omega_c}{s + \omega_c} \quad (2.11)$$

Where, $K_p$, $K_i$, *and* $T_i = \frac{K_p}{K_i}$ are the proportional gain, integral gain, and integral time constant, respectively, and $\omega_c$ is the cut-off frequency.

The PI controller gains can be calculated based on the symmetric or magnitude optimum criterion [18]. The proportional action ($K_p$) reacts to the current error and provides an immediate response. The integral action ($K_i$) accumulates past errors and ensures that the output reaches and stays at the setpoint over time. The PI controller does not include a derivative ($K_d$) term, making it less sensitive to noise compared to a PID controller.

## 2.4 Fuzzy Logic-Based Controller with Grid Connected Inverter

### 2.4.1 Fuzzy Logic Controller

A Fuzzy Logic Controller (FLC) is an intelligent control system that can handle imprecise or uncertain inputs, making it highly effective for nonlinear systems. Unlike traditional binary logic systems, which operate only with discrete values (0 or 1), fuzzy logic can work with a range of values between 0 and 1. This enables smooth and adaptive control, even in complex and dynamic environments. The components of Fuzzy Logic control system and their working are described as below:

a) Fuzzification: Converts numerical (crisp) input values into fuzzy values using membership functions. In the given system, the inputs are Error and Change in Error derived from voltage and current measurements at the Point of Common Coupling (PCC). Membership functions define linguistic variables like Negative Large (NL), Negative Medium (NM), Negative Small (NS), Zero (Z), Positive Small (PS), Positive Medium (PM), and Positive Large (PL).

b) Inference System: This system applies logical reasoning based on a predefined rule base to determine the system's response. The rule base, shown in Table 2.2, determines how the controller reacts to different combinations of error and change in error. This uses Madani’s Rule-Based Technique for decision-making.

c) Defuzzification: It converts the fuzzy output values back into a crisp numerical value and determines the final control action (duty cycle for pulse width modulation in power converters).

### 2.4.2 Fuzzy Logic Control Process

The fuzzy logic control process mentioned in [19] are described as below:

1. Inputs Calculation: The inputs Error (E) and Change in Error (ΔE) are computed based on voltage and current variations at the PCC and the small variations are taken as crisp inputs.
2. Fuzzification: Error and change in error are converted into fuzzy terms

using membership functions.

3. Inference System: Uses the rule base (Table 2.2) to determine the appropriate fuzzy control action.
4. Defuzzification: Converts the fuzzy output into a specific duty cycle for controlling the system.

*Table 2.2: Rule base for fuzzy controller in current regulator*

| **Change in Error** | **PL** | **PM** | **PS** | **Z** | **NS** | **NM** | **NL** |
|---|---|---|---|---|---|---|---|
| NL | PL | PL | PL | PM | PM | PS | Z |
| NM | PL | PL | PM | PM | PS | Z | ZS |
| NS | PL | PM | PS | Z | NS | NM | NL |
| Z | PL | PM | PS | Z | NS | NM | NL |
| PS | PM | PS | Z | NS | NM | NL | NL |
| PM | PS | Z | NS | NM | NM | NL | NL |
| PL | Z | NS | NM | NL | NL | NL | NL |

### 2.4.3 Limitations with Fuzzy Logic Control Process

While Fuzzy Logic Controllers (FLCs) offer significant advantages, they also come with several challenges and limitations, particularly in real-world applications. The several limitations of FLC are:

1. Complex Rule Base Design: As the number of input variables increases, the number of rules grows exponentially, making it difficult to manage and optimize and unlike traditional controllers, which rely on mathematical models, FLCs depend on a set of heuristic rules.

2. Difficulty in Tuning and Optimization: Unlike PID controllers, where gains can be adjusted mathematically, FLC tuning is mostly trial-and-error, determining the optimal membership functions, rule base, and defuzzification method is time-consuming and Lack of systematic approaches for adjusting scaling factors and membership function parameters.

3. Lack of a Universal Mathematical Model: Unlike PID controllers, which have

well-defined transfer functions, FLCs do not have a universal mathematical representation. This makes it hard to analyze system stability using traditional control theory tools like Bode plots or root locus.

So, Researchers have proposed hybrid controllers (e.g., Fuzzy-PID, Adaptive Neuro-Fuzzy Inference System (ANFIS)) to improve stability and mathematical formulation.

## 2.5 Multilevel Inverter

The concept of multilevel inverters (MLIs) was first introduced in 1975 by R. H. Baker and L. H. Bannister to increase inverter power ratings while reducing individual device ratings by incorporating multiple voltage levels. MLIs generate a continuous sinusoidal waveform by utilizing multiple DC voltage levels as input, making them a superior alternative to traditional two-level inverters. Their advantages include reduced harmonic distortion, simplified filtering requirements, improved sinusoidal output waveforms, and lower voltage stress (dv/dt) on switching devices. Due to their ability to ensure high power quality, MLIs are widely applied in high-voltage DC transmission, renewable energy conversion, distributed generation (DG) systems, and uninterruptible power supplies. Multilevel inverters are classified into Current-Source Inverters (CSI) and Voltage-Source Inverters (VSI). However, CSI-based MLIs can result in high fault currents during short circuits, potentially damaging connected equipment. As a result, Voltage-Source MLIs are more commonly used due to their enhanced reliability and performance [39].

## 2.6 LCL Filters

The designing an LCL filter for a 3-phase inverter is essential to reduce high-frequency switching harmonics and provide a smooth sinusoidal output voltage or current. To guarantee optimum performance, a few important factors need to be considered while designing an LCL filter. Current ripple is one important component that is managed by the inverter-side inductance to keep it within 10% of the nominal amplitude and guarantee smooth current flow. The capacitance and inductance values also affect the filter size and need to be carefully chosen to strike a balance between performance and physical limitations. Switching ripple attenuation is another crucial component since grid compliance requires the LCL

filter to efficiently suppress high frequency switching harmonics produced by the inverter. But adding a capacitor creates a resonance problem since it may interfere with the grid impedance and lead to stability issues.

Damping devices are needed to minimize this; in this instance, passive damping is accomplished by connecting a series resistor to the capacitor. The overall design procedure and mathematics are as mentioned in [15]. The base Impedance is calculated as,

$$Z_b = \frac{U_n^2}{S_n} \tag{2.12}$$

Where, $U_n$ = Line-to-line RMS voltage and $S_n$ = Rated apparent power

The base capacitance is calculated as,

$$C_b = \frac{1}{\omega_b Z_b} \tag{2.13}$$

Where $\omega_b$ = angular frequency = $2\pi f$

The inverter side inductance is calculated as,

$$L_i = \frac{\Delta I_{L_{\max}} \times 16 f_s}{V_{DC}} \tag{2.14}$$

And the current ripple constraint is given by,

$$\Delta I_{L_{max}} = 0.1 \times \frac{P_n}{\frac{U_n}{\sqrt{2}}} \tag{2.15}$$

Where, $P_n$ = Nominal active power

$f_s$ = Switching frequency

And $V_{dc}$ = DC link voltage

Based on the power factor variation constraint of (5%), the filter capacitance is given by,

$$C_f = 0.05 C_b \tag{2.16}$$

The grid side inductance is calculated as,

$$L_g = r \times L_i \tag{2.17}$$

Where, r is a scaling factor (typically between 1 to 3).

The resonance frequency must be Far from the grid frequency ($f_g$) and less than half of the switching frequency $\frac{f_s}{2}$. The resonance frequency of LCL filter is given by,

$$f_{res} = \frac{1}{2\pi}\sqrt{\frac{(L_g+L_i)}{L_g L_i C}} \quad (2.18)$$

To suppress oscillations, a series damping resistor $R_d$ is added to the capacitor. The value of $R_d$ is calculated as,

$$R_d = \frac{1}{3\omega_{res} C} \quad (2.19)$$

Where, $\omega_{res} = 2\pi f_{res}$ (2.20)

## 2.7 Some Achievements on PQ Improvement in GC PV

In recent years, several prominent companies have made significant advancements in improving power quality (PQ) in grid-connected photovoltaic (PV) systems. Here are some notable achievements:

1. Enel Green Power has been at the forefront of integrating advanced energy storage solutions to enhance PQ in their solar PV installations. In March 2024, they activated Europe's largest vanadium redox flow battery at the Son Orlandis solar PV plant in Mallorca. This integration aims to stabilize the grid by effectively managing the intermittent nature of solar energy, thereby improving overall power quality [27].

2. Vikram Solar has achieved significant milestones in enhancing PQ within grid-connected PV systems. In 2023, they increased their module production capacity to 3.5 GW and received accreditation from NABL in accordance with ISO/IEC 17025:2017, becoming the second solar company in India and the first in Eastern India to achieve this. They also launched n-type monocrystalline cells with Tunnel Oxide Passivated Contact (TOPCon) and heterojunction (HJT) PV modules, which offer higher efficiency and better performance, contributing to improved power quality in PV installations [28].

3. China has made significant strides in deploying smart grid technologies to enhance PQ in its rapidly expanding PV installations. The State Grid Corporation of China (SGCC) has invested heavily in smart meters, with plans to equip all users by 2014. By 2011, SGCC had deployed 45 million smart meter units, aiming for a total of 330 million units, enhancing monitoring and management of power quality across the grid [29].

4. In Nepal, Nuwakot Solar Power Station, located in the Nuwakot District, this is Nepal's largest solar power plant, owned by the Nepal Electricity Authority

(NEA). The plant connects to the 66 kV sub-station of the Devighat Hydropower Station, enhancing PQ by stabilizing voltage levels and reducing dependence on hydroelectric power during dry seasons [30]. Butwal Solar PV Project: Commissioned in October 2020, this 8.5 MW plant operates in the Rupandehi District. It supplies energy to the 33 kV Butwal Substation, contributing to improved PQ by providing a stable and renewable energy source to the local grid [31]. Additionally, research efforts in Nepal, such as the study on "Power Quality Enhancement Strategy in Grid Connected Dual Voltage Source Inverters Supplying Various Loads," have focused on implementing control algorithms based on instantaneous symmetrical component theory (ISCT). These strategies aim to reduce Total Harmonic Distortion (THD) below 3%, ensuring stable and reliable operation of interconnected grids [32].

## 2.8 Review of Literatures

Several papers basically related with MPPT, Multilevel Inverter, ML based Controllers and Filters for PQ improvements in GC systems has been studied and summarized below.

The paper [33] provides the comparison between different MPPT algorithms. As discussed in [33], when MPPT is reached, Perturb and observe (P and O) algorithm will oscillate around maximum power point (MPP) and will search in the wrong direction by considering only power variations. Unlike P and O, Incremental Conductance will resolve the problem of power variation based on change in power with respect to change in voltage $\left(\frac{dp}{dv}\right)$ but there is the slow convergence in the maximum power and problem with the partial shading conditions. Another iterative technique, Genetic Algorithm based technique implemented in [34] improves the convergence, rapidity, and accuracy of the PV system and can also efficiently track the global MPP, which is very useful for partial shading. A single current sensor-based hybrid MPPT method combining artificial bee colony (ABC) and hill climbing (HC) algorithms tracks the Global maxima efficiently under mismatch insolation conditions [35]. A velocity of particle swarm optimization-based Levy flight (VPSO-LF) based Global MPPT method for PV systems under partial shading conditions achieving faster convergence and superior performance is proposed in [36]. Fuzzy logic (FL) provides the best balance of speed, accuracy, and stability, while ANN (artificial neural network) has been based on three meta-heuristic

algorithms, including genetic algorithm (GA), particle swarm optimization (PSO) algorithm, and imperialist competitive algorithm (ICA) to provide the fast convergence however, this method is more complex for implementation [37]. CFFNN model for PV power prediction using GA, achieving superior accuracy and faster training/testing compared to classical feed-forward neural network (FFNN), classical CFNN, and FFNN-GA, making it a recommended approach for PV output forecasting [38]. In this study, a Cascaded Feed Forward Neural Network (CFFNN)-based Maximum Power Point Tracking (MPPT) algorithm is used to track the Maximum Power Point (MPP) which is a machine learning-driven approach designed to optimize the performance of photovoltaic (PV) systems by dynamically adjusting the operating point to extract maximum power. This method leverages the learning capabilities of neural networks to handle nonlinearities, environmental variations, and rapid fluctuations in irradiance and temperature.

Traditional two-level inverters generate square waves, which require additional filtering to obtain sinusoidal waveforms suitable for grid integration. Even more, the traditional converters rating power is limited to the rated power of the used semiconductor devices and the allowed switching frequencies [20]. Power-frequency transformers and AC filters are used in renewable systems to step up the voltage and minimize THD, but these components add bulk, cost, and complexity [21]. New power semiconductor devices enable advanced converter topologies like Modular Multilevel Cascaded (MMC) converters, which can handle medium and high voltage applications efficiently [22]. The proposed three-phase Integrated Module Multilevel Inverter (IMMLI) in [23] achieves high output levels with fewer components using series-connected basic blocks while ensuring low total stress voltage (TSV), improved efficiency, and cost reduction, with multi-carrier PWM for optimal AC power quality and a high-frequency magnetic-link for balanced DC sources. A new 11-level multilevel inverter topology with eight switches and two uneven input sources for achieving the low harmonic distortion is presented in [24]. Renewable energy resource integrated multilevel inverter using evolutionary algorithms are employed to reduce overall harmonic distortion [25]. However, there is the lag of harmonic analysis while the

varying irradiances and temperature at the same period. Furthermore, the higher the number of switches operating with maximum voltage stress (MVS), the higher the switching losses, and the lower the application compatibility of the inverter for high

power systems [26]. Therefore, creating a perfect trade-off between the design, and the corresponding cost, TSV, power quality and efficiency of an MLI may be considered as an essential objective. Common issues in above mentioned Multilevel Inverters (SCMLIs) include low reliability, reduced durability, large volume, bulky weight, high inrush current, and significant capacitor ripple voltage losses, where the use of multiple capacitors further increases the inverter's overall size and weight.

Therefore, 9 level ACMLI with five medium voltage MOSFETs, each having four PV modules is implemented here to improve the power quality issues. The SPWM technique is used to generate the pulses in the described multilevel inverter. The H-bridge would be used to design the recommended multilevel inverter in two steps as DC-DC and DC- AC.

# 3. RESEARCH METHODOLOGY

This chapter presents the research methodology that is carried out during our research works in three sections which is summarized as below.

## 3.1 Genetic Algorithm Based MPPT

The genetic algorithm leverages short-circuit current ($I_{sc}$) and open-circuit voltage ($V_{oc}$) to quickly adapt to climatic changes and identify the Maximum Power Point (MPP) without perturbation steps, using Genetic Algorithms to ensure diverse solutions and avoid local optima. It compares performance with Perturb and Observe (PO) and Incremental Conductance (IC) methods, using a population-based approach to track the MPP globally and reduce power oscillation. The main concept is to perform genetic transformations - selection, crossover, mutation, and insertion—on a population of individuals to ultimately identify an optimal individual representing the maximum of the fitness function. The flowchart in Figure 3.1 outlines the algorithm's steps.

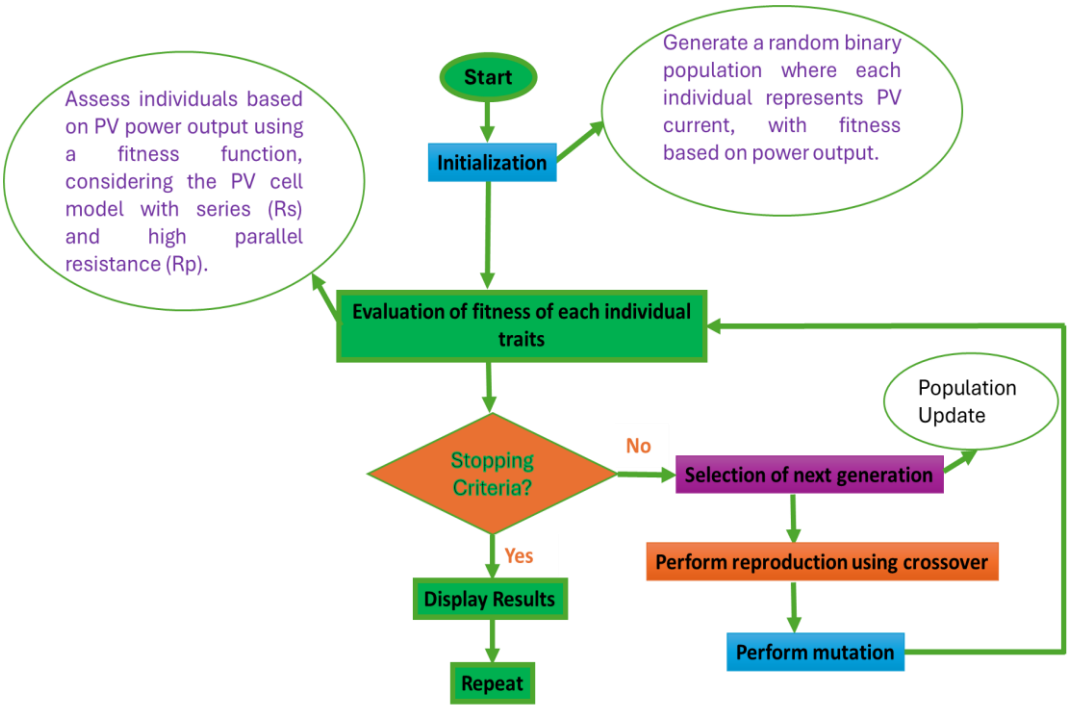


Fig. 3.1. Flowchart of Genetic Algorithm

Step 1: Initialization

The binary matrix that forms the initial population in our algorithm is randomly

generated and consists of N individuals, where each individual represents photovoltaic current and is coded using S bits with Imax = Isc. The power (fitness) of each individual is used to evaluate the created population.

Step 2: Evaluation

The process of evaluation is crucial as it determines the survival of the fittest individual. The fitness function plays a significant role in this process by optimizing the individual for the maximum value of its fitness function, which is a positive function. In our approach, we utilize the PV power as the fitness function, ensuring that the optimal individual generates the maximum power output. Each individual, representing the PV current, is evaluated based on its corresponding power output.

$$P = V.\ I \tag{3.1}$$

The cell model, shown by the circuit in Figure 3.2, is used to evaluate the power of each individual (fitness function), where Rp and Rs are the series and parallel resistances of the cell, respectively [16].

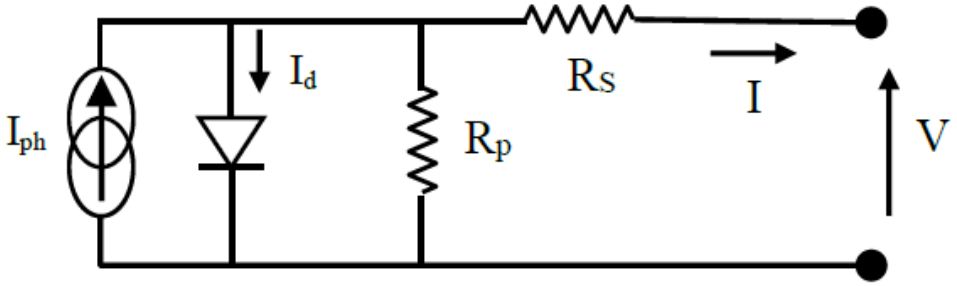


Fig. 3.2: Schematic Diagram of Solar PV Cell

Usually, the value of Rp is very high, so the equation for the output current can be given by:

$$I = I_{ph} - I_d \tag{3.2}$$

With:

$$I_d = I_{rs}\left[e^{\left(\frac{q(V+R_S I)}{kTA}\right)} - 1\right] \tag{3.3}$$

Where: $I$ = Output Current (A), $V$ = Output Voltage (V), $I_d$ = Current through the intrinsic diode, $I_{ph}$ = Cell photocurrent, $I_{rs}$ = Cell reverse saturation current, q = charge of an electron, $k$ = Boltzmann's Constant, $A$ = The p-n junction ideality factor, $T$ = Cell Temperature (K), $R_s$ = Series Resistance of the cell

Making the approximation that $Iph \sim Isc$ where Isc is short-circuit current becomes [10]:

$$I = I_{sc} - I_{rs}[e^{\left(\frac{V+R_S I}{V_T}\right)} - 1] \tag{3.4}$$

Where:

$$V_T = \frac{kTA}{q} \tag{3.5}$$

At open circuit I = 0 and V = $V_{oc}$, with $V_{oc}$ is open-circuit voltage; Using (3.4), we can write:

$$I_{rs} = \frac{I_{sc}}{e^{\frac{V_{oc}}{V_T}} - 1} \tag{3.6}$$

Using (3.4) and (3.6), the output voltage equation of the cell will be:

$$V = V_T ln\left[\left(1 - \frac{I}{I_{sc}}\right)\left(e^{\left(\frac{V_{oc}}{V_T}\right)} - 1\right) + 1\right] - R_s I \tag{3.7}$$

Finally, the power equation can be given with (3.1) and (3.7):

$$P = \left(V_T ln\left[\left(1 - \frac{I}{I_{sc}}\right)\left(e^{\left(\frac{V_{oc}}{V_T}\right)} - 1\right) + 1\right] - R_s I\right) * I \tag{3.8}$$

By applying the given equation, the power (fitness function) of each individual is computed, and this value is utilized in genetic operations to generate a new population (generation). The newly created population is then inserted into the parent population based on their respective fitness function values.

Step 3: Generic Operations

a. Selection

In the selection operation of genetic algorithms, individuals are chosen to be parents for the next generation based on their fitness, with fitter individuals having a higher chance of selection. The roulette wheel selection method is used to ensure that individuals with better fitness values are more likely to pass on their genetic material.

b. Crossover

Crossover combines genetic material from two parent individuals to create offspring, mimicking natural genetic recombination. By exchanging genetic information at randomly chosen points, it introduces diversity and potentially combines beneficial traits, exploring new regions in the search space.

c. Mutation

Mutation introduces random changes to an individual's genetic material after crossover, such as flipping bits or altering values, to maintain genetic diversity and avoid local optima. This process allows for small variations in the population, helping to explore new potential solutions.

d. Insertion

The new population will be merged with the existing one, replacing individuals with the lowest fitness function values. As a result, the new generation will consist of the

same number of individuals as before.

e. Stopping Criteria

The program generates new individuals that are optimized for the problem at hand. The execution of the program concludes after a predetermined number of iterations, ensuring a consistent runtime. Extensive testing was conducted to determine an iteration count that strikes a balance between achieving optimal results and minimizing processing time.

## 3.2 Solar PV System Design and Modelling with CFFNN MPPT

Spectrum The designing and modelling of a Solar PV system consists of an efficient Cascaded Feed Forward Neural Network (CFFNN) MPPT along with the Boost Converter. The CFFNN is implemented to enhance the performance of PV system. One important aspect of SPV system modelling is the creation of a test cell to measure the values of $I_{sc}$ and $V_{oc}$, which can then be used to accurately model the system's behaviour. Additionally, the modelling of the PV system and the development of a new MPPT system are essential components of the design process. Figure 3.2 represents the electrical model of a PV cell consisting of a photocurrent and a diode describing the properties of the semiconductor. A series resistance Rs represents an internal resistance, and a parallel resistance Rp showing a leakage current. The mathematical equation expressing the charging current can be given as [17]. Figure 3.3. presents the overall system for MPPT system implemented in this case.

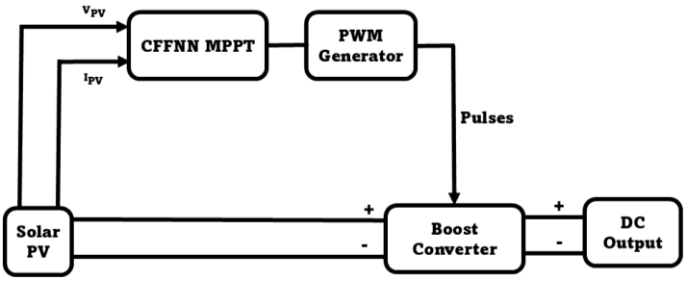


Fig. 3.3: CFFNN based MPPT with Boost Converter

A Cascaded Feed-Forward Neural Network (CFNN) is an extension of the conventional Feed-Forward Neural Network (FFNN), where additional connections exist between the input (contribution) layer and each subsequent layer, including the output layer. This structure improves information flow, helping the network to learn complex nonlinear relationships more effectively. In a three-layer CFNN: The

output layer is directly connected to both the input layer and the hidden layers, and this additional connectivity helps preserve input information throughout the network, enhancing its ability to approximate complex functions. The output of a CFNN with one hidden layer is expressed as in Eq. (3.9).

$$y = \sum_{i=1}^{n} f_i w_{ii} x_i + f_0\left(\sum_{j=1}^{n} w_j^o f_j^h\left(\sum_{i=1}^{n} w_{ji}^h x_i\right)\right) \quad (3.9)$$

Where, y is the output (predicted value), $x_i$ are the input features (contribution layer neurons), $w_{ii}$ are the direct weights connecting the input layer to the output layer, ${w_{ji}}^h$ are the weights connecting the input layer to the hidden layer, ${w_j}^0$ are the weights from the hidden layer to the output layer, $f_0$ and ${f_j}^h$ are the activation functions. When bias $(b_i)$ is introduced to enhance the performance of system, the equation modifies to:

$$y = \sum_{i=1}^{n} f_i w_{ii} x_i + f_0\left(w_b + \sum_{j=1}^{n} w_j^o f_j^h\left(b_i + \sum_{i=1}^{n} w_{ji}^h x_i\right)\right) \quad (3.10)$$

CFFNN is well-suited for time-series data processing. In such cases, the input neurons represent the lagged time-series values as:

$$x_t = f\left(x_{t-1}, x_{t-2}, \ldots, x_{t-p}\right) \quad (3.11)$$

The output neuron predicts the current value $x_t$. CFFNN is applied to MPPT in a photovoltaic (PV) system. The input features are $V_{PV}$ and $I_{PV}$ and the output is duty cycle for the DC-DC converter. Thus, the CFFNN learns the relationship between PV voltage, current, and the optimal duty cycle, allowing real-time adjustment to track the MPP. The CFNN architecture model is as shown in figure 10 which consists of:

a. Input layer which is also called contribution layer having two neurons whose main role is to capture real-time PV parameters and sends the input features to the hidden layers for processing

b. hidden layers also called concealed layers which can process the input data, capturing the complex nonlinear relationships between voltage, current, and the optimal duty cycle. The hidden layers are sub grouped into six layers: layer 1 having twenty neurons, layer 2 having thirty neurons, layer 3 having thirty neurons and layer 4 having twenty neurons, layer 5 having twenty neurons and layer 6 having five neurons. The activation functions used in the hidden layers are, Rectified Linear Unit and sigmoid function. The rectified linear unit (RLU) and sigmoid functions can be represented as in eq 3.12 and 3.13.

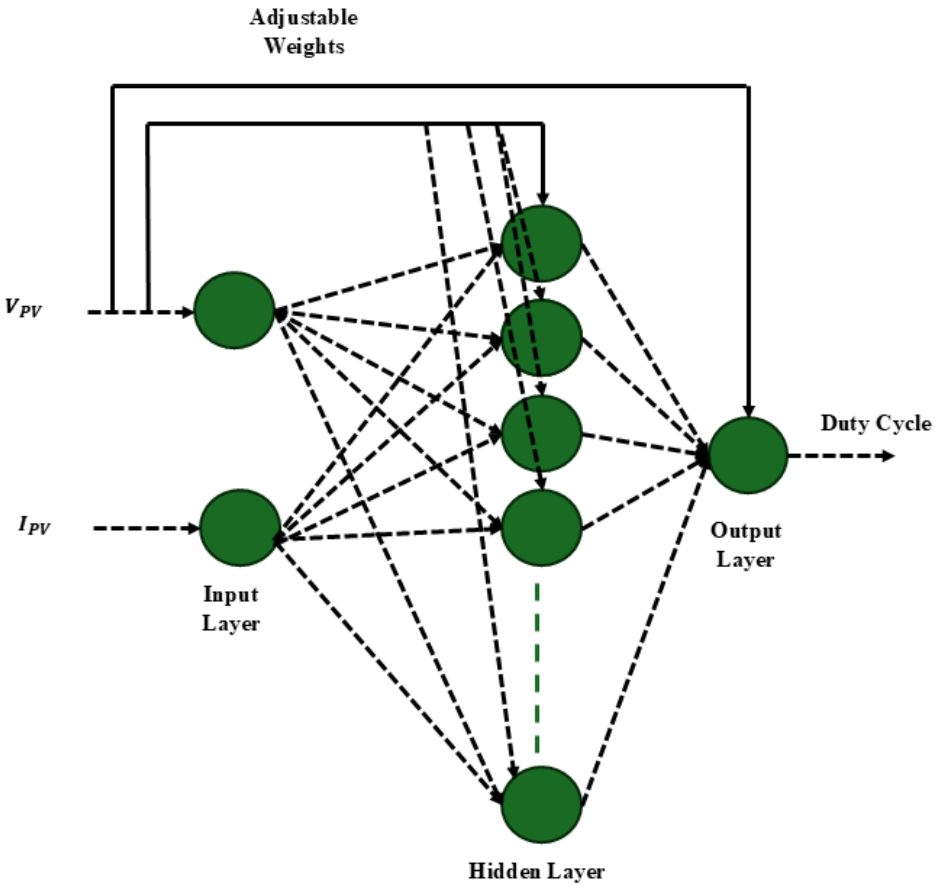


Fig. 3.4: CFFNN Network Architecture

The output layer also called production layer which can provide the duty cycle which include linear activation function.

$$RLU(x) = max(0, x) \tag{3.12}$$

and

$$Sigmoid(x) = \frac{1}{1+e^{-x}} \tag{3.13}$$

## 3.3 Overall System Design and Modelling

The block diagram for the overall system is as shown in figure 3.5. The figure represents a grid-connected ANFIS based Cascaded Multilevel Inverter (CMLI) system, designed to integrate multiple DC sources into a microgrid and further synchronize it with a microgrid. The system consists of multiple stages, including DC-AC conversion, filtering, voltage transformation, and grid integration. The output of PV MPPT is fed to the boost converter and output of the boost converter is utilized as DC voltage source in the ACMLI system. The LCL filter is implemented in the system to reduce the harmonics in the output of inverter. The 19 bus distribution loads (linear as well as non-linear loads) are supplied from the

output of the inverter. The 11/0.4 KV step up transformer is used to increase the voltage level. A transmission line is used to feed the output of CMLI into 100 MVA, 11KV three phase which is treated as a microgrid. To generate the switching pulses of the inverter, ANFIS based current regulators are used.

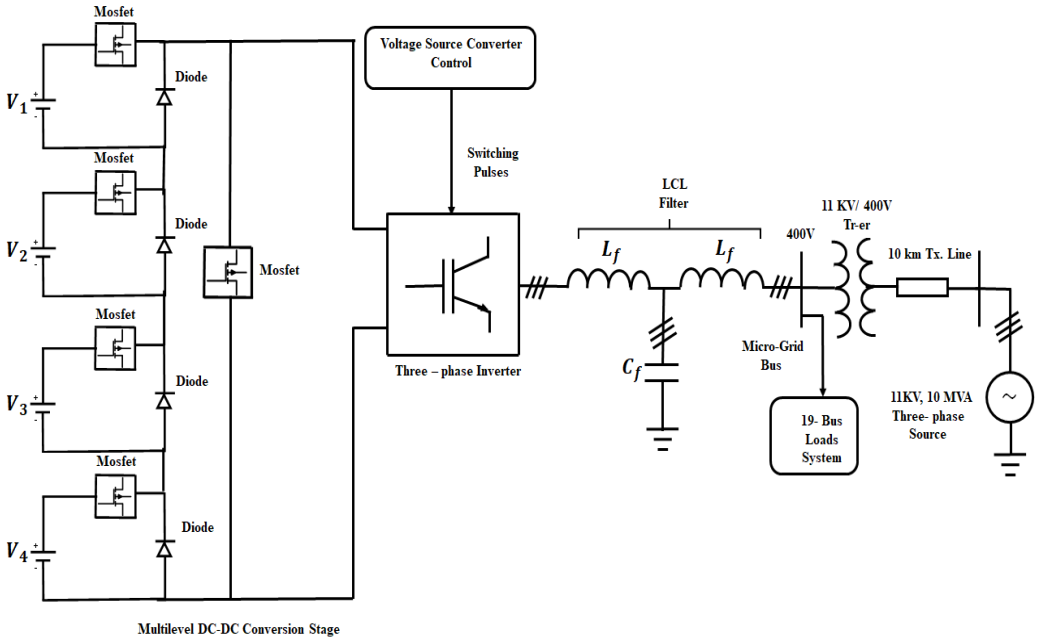


Fig. 3.5. ANFIS Based Multilevel GCI with 19- bus DS

The diagram represents a 2-stage 9-level Cascaded Multilevel Inverter (CMLI), which consists of two stage of power conversion- DC-DC power conversion and DC- AC power conversion. This CMLI consists of four switches each powered by an independent DC voltage source ($V_1$, $V_2$, $V_3$, $V_4$). The function of this inverter is to generate a multi-stepped AC output voltage by switching different DC levels in sequence. A 9-level inverter requires four separate DC sources (as shown in the diagram). The output voltage is synthesized by summing up different voltage levels, providing a staircase waveform with reduced harmonics. The possible output voltage levels are:

$$V_{out} = \{-V_{dc}, -\frac{3V_{dc}}{4}, -\frac{V_{dc}}{2}, -\frac{V_{dc}}{4}, 0, \frac{V_{dc}}{4}, \frac{V_{dc}}{2}, \frac{3V_{dc}}{4}, V_{dc}\} \quad (3.14)$$

This means that there are 9 different levels in the output waveform. Each switch contributes to the total output voltage by switching ON/OFF different voltage sources. The inverter follows the below as in table 6 switching sequence to generate a stepped AC waveform. Here, "ON" means the MOSFETs are conducting in a forward direction, "Reverse ON" means the MOSFETs are conducting in a reverse polarity to generate negative voltage and "OFF" means the MOSFETs are not

conducting.

*Table 3.1: Switching States of Each MOSFETs*

| Output Voltage (Vout) | MOSFET 1 | MOSFET 2 | MOSFET 3 | MOSFET 4 |
|---|---|---|---|---|
| **+Vdc** | ON | ON | ON | ON |
| **+3Vdc/4** | ON | ON | ON | OFF |
| **+Vdc/2** | ON | ON | OFF | OFF |
| **+Vdc/4** | ON | OFF | OFF | OFF |
| **0V** | OFF | OFF | OFF | OFF |
| **-Vdc/4** | Reverse ON | OFF | OFF | OFF |
| **-Vdc/2** | Reverse ON | Reverse ON | OFF | OFF |
| **-3Vdc/4** | Reverse ON | Reverse ON | Reverse ON | OFF |
| **-Vdc** | Reverse ON | Reverse ON | Reverse ON | Reverse ON |

## 3.4 ANFIS Controller Based Multilevel Grid Connected Inverter

ANFIS Controller Based Multilevel Inverter is connected a microgrid having linear as well as non-linear loads with 19 bus system as illustrated in figure 3.6. A multilevel inverter (MLI) plays a vital role in integrating renewable energy sources with the grid due to its ability to generate high-quality sinusoidal voltage with lower Total Harmonic Distortion (THD). The Adaptive Neuro-Fuzzy Inference System (ANFIS) is an intelligent control technique that combines artificial neural networks (ANN) and fuzzy logic to provide an adaptive and robust control approach. In a grid-connected system, ANFIS-based control enhances the inverter's performance by ensuring proper synchronization, power quality, and dynamic response to varying grid conditions. The structure of ANFIS based MLI system consists of a renewable energy source, such as photovoltaic (PV), which generates DC electricity. A DC-DC converter is used to regulate the DC voltage and ensure a stable input for the inverter. The multilevel inverter, which can be based on topologies like Cascaded H-Bridge, converts the regulated DC voltage into an AC waveform suitable for grid integration. To optimize switching control and improve system performance, an ANFIS controller is employed, providing adaptive and intelligent regulation. Additionally, a Phase-Locked Loop (PLL) ensures proper grid synchronization by maintaining the phase and frequency alignment of the inverter output with the grid. Finally, a grid interface consisting of filters and transformers ensures compliance with grid standards, reducing harmonics and ensuring high power quality.

The overall control strategy used for generating the switching pulses is as shown in

figure 12. This block diagram represents a 7-layered ANFIS-based controller for a grid-connected inverter system, which ensures efficient control of active and reactive power while maintaining synchronization with the grid. The system integrates multiple components, including a Phase-Locked Loop (PLL), abc-dq transformation, PI controller for outer voltage loop control, ANFIS-based current and voltage controllers, reference voltage computation, and Sinusoidal Pulse Width Modulation (SPWM). The three-phase Phase-Locked Loop (PLL) system is responsible for extracting the grid frequency and phase angle, which is crucial for achieving synchronization. The grid voltage $(V_{g,abc})$ is fed into the PLL, which tracks the phase angle $(\omega t)$ and generates the required frequency reference $(f)$.This phase angle is then used to transform three-phase voltage and current components from the abc reference frame to the dq reference frame using an abc to dq transformation block. This transformation simplifies the control process by converting AC signals into DC-like quantities, allowing for better regulation and control. The DC-link voltage regulation is a key part of the system, ensuring that the inverter maintains a stable voltage level. The measured DC voltage $(V_{dc,meas})$ is compared with the reference voltage $(V_{dc,ref})$, and the error is processed by a PI controller. The outer control loop is responsible for generating the reference current $(i_{d,ref})$ for the inner control loop which is used for active power regulation. To ensure the current remains within a safe operating range, a limiter is typically applied to the controller output. Furthermore, the time constant of the outer control loop is set higher than that of the inner loop to maintain stability. A stable DC-link voltage ensures that the inverter can provide a smooth and regulated AC output to the grid. When the inner loop settles $i_{d,ref} = i_d$; the inner loop can be just treated as a unity gain.

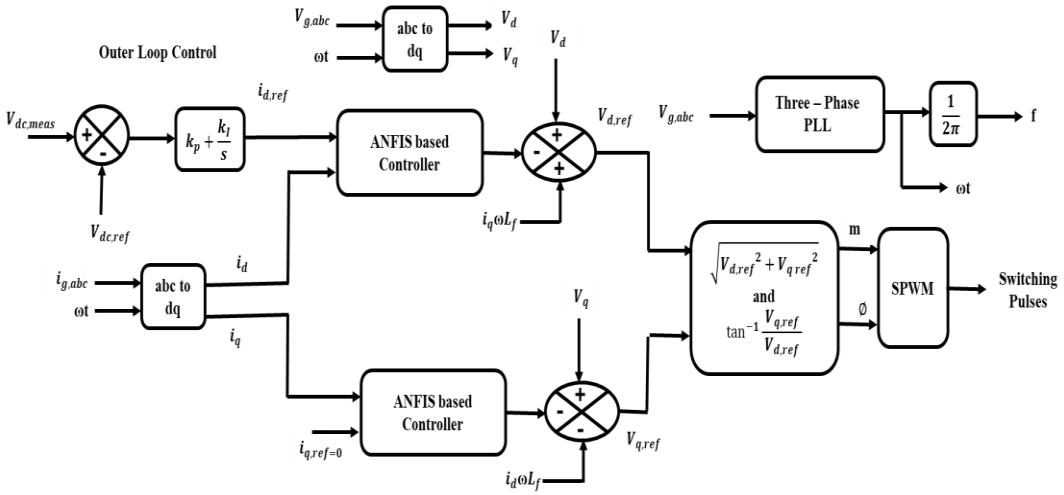


Fig. 3.6. ANFIS Based MLI Control

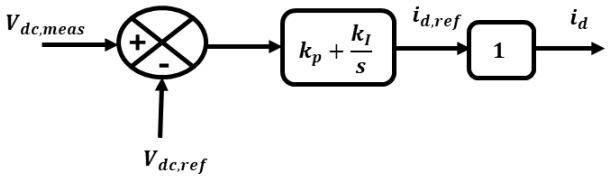

Fig. 3.7. Resultant Open Loop TF

The resultant open loop transfer function can be drawn as in figure 10.

The DC voltage, $v_{dc}$, shown in figure 3.7 and 3.8 is calculated by the following equations. The capacitor current is given by,

$$i_C = \mathrm{i} - i_{dc} \tag{3.15}$$

and

$$i_C = C\frac{dv_{dc}}{dt} \tag{3.16}$$

Therefore, $C\frac{dv_{dc}}{dt} = i - i_{dc}$ (3.17)

The transfer function to obtain $v_{dc}$ is,

$$v_{dc} = \frac{i\,(s) - i_{dc}\,(s)}{Cs} \tag{3.18}$$

The DC current $i_{dc}$ is related to direct axis current $i_d$ as

Power, $P = i_{dc} \times v_{dc} = v_g \times i_d$ (3.19)

So, $i_{dc} = \frac{v_{gd}}{v_{dc}} \times i_d$ (3.20)

Assuming, $v_g$ and $v_{dc}$ are constants, the relation between $i_d$ and $i_{dc}$ by a gain $k$ as,

$$i_{dc} = k \times i_d \tag{3.21}$$

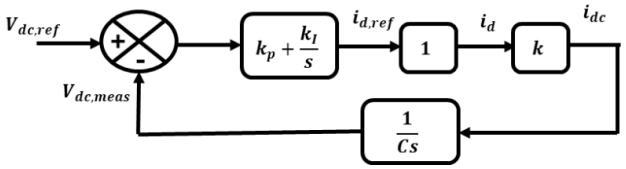


Fig. 3.8. Resultant Closed Loop TF

By using the transfer function obtained from the equations represented above, we can calculate the value of $k_p$ and $k_I$ for the outer voltage loop controller. The $k_p$ and $k_I$ obtained based on this method are 10.0031579 and 812.235575 respectively. To enhance the performance of current regulation, the system employs 7-layered ANFIS-based controllers. These controllers use Adaptive Neuro-Fuzzy Inference Systems (ANFIS), which combine artificial neural networks (ANN) and fuzzy logic to provide adaptive and nonlinear control as in figure 3.6.

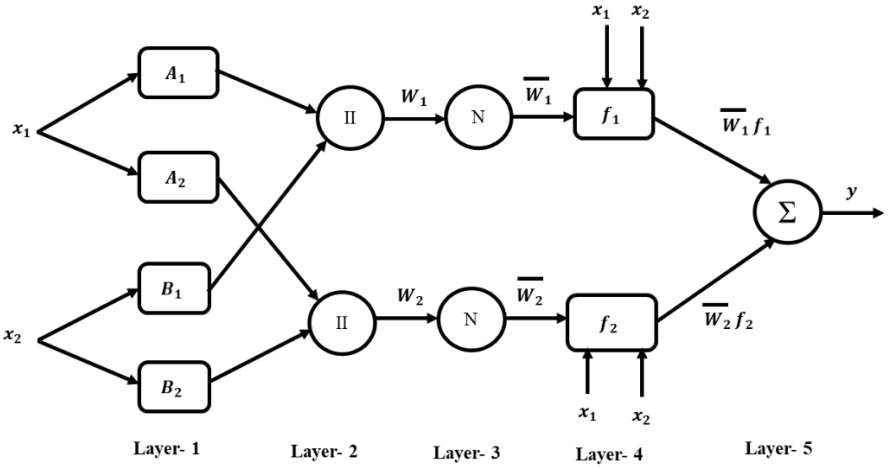


Fig. 3.9. Architecture of two inputs- one output Sugeno ANFIS with two rules

The given diagram represents a five-layer ANFIS architecture, which combines fuzzy logic and neural networks for adaptive learning and control. In Layer 1, the system applies fuzzy membership functions to the input variables. Each neuron in this layer represents a membership function corresponding to a fuzzy rule. The inputs $x_1$and $x_2$ are mapped to fuzzy sets represented by $A_1$ , $A_2$ for voltage and $B_1$ , $B_2$ for current. These membership function evaluate the degree to which the input belongs to a particular fuzzy category. Layer 2 performs the fuzzy AND operation to determine the weightage strength of each rule. The outputs of the membership functions from Layer 1 are multiplied to compute the rule strength. Mathematically, the rule strengths are given by:

$$w_1 = A_1(x_1) \cdot B_1(x_2) \tag{3.22}$$

and $w_2 = A_2(x_1) \cdot B_2(x_2)$ (3.23)

In Layer 3, the system normalizes the rule strengths to ensure that their total sum is

equal to one. This is done using the equations

$$\overline{w_1} = \frac{w_1}{w_1+w_2} \tag{3.24}$$

and $\overline{w_2} = \frac{w_2}{w_1+w_2}$ (3.25)

Normalization ensures that the influence of each rule is proportionally distributed, making the control system more stable. Layer 4 represents the adaptive consequence layer, where each neuron applies a linear function to compute the rule output. Two rules are associated with a linear equation of the form

$$f_1 = p_1 V_g + q_1 i_g + r_1 \tag{3.26}$$

and $f_2 = p_2 x_1 + q_2 x_2 + r_2$ (3.27)

where $p$, $q$ and $r$ are trainable parameters. The rule outputs are then weighted by their normalized firing strengths, resulting in,

$$\overline{w_1} f_1 = \frac{w_1}{w_1+w_2} f_1 \tag{3.28}$$

and

$$\overline{w_2} f_2 = \frac{w_2}{w_1+w_2} f_2 \tag{3.29}$$

Finally, Layer 5 aggregates the weighted rule outputs to produce the final crisp output using a weighted summation. The final output is computed as,

$$y = \sum \overline{w_i} f_i = \overline{w_1} f_1 + \overline{w_2} f_2 \tag{3.30}$$

This layer aggregates all the rule outputs to generate a sharp value. The given table 3.2 represents the rule base of an Adaptive Neuro-Fuzzy Inference System (ANFIS), which is a hybrid system that combines the learning capability of neural networks with the reasoning power of fuzzy logic. This rule base is an essential component of ANFIS, as it defines how input variables are mapped to output variables based on fuzzy logic rules. Functions of each component are described below:

*Table 3.2: Rule Base of ANFIS*

| | **In2mf1** | **In2mf2** | **In3mf3** |
|---|---|---|---|
| **In2mf1** | OPT1mf1 | Out1mf2 | Out1mf3 |
| **In2mf2** | OPT1mf4 | Out1mf5 | Out1mf6 |
| **In3mf3** | Out1mf7 | Out1mf8 | Out1mf9 |

1. Input Membership Functions (MFs)
    - The row labels (In2mf1, In2mf2, In3mf3) represent different membership functions of Input 1 (In2).

- The column labels (In2mf1, In2mf2, In3mf3) represent different membership functions of Input 2 (In3).
- The combination of these membership functions determines which rule will be applied in the fuzzy inference system.

2. Output Membership Functions (MFs)

- The values inside the table (OPT1mf1, Out1mf2, etc.) are the output membership functions that correspond to a particular rule.
- These represent the fuzzy output associated with a specific combination of inputs.

This ANFIS rule base uses a Sugeno-type fuzzy inference system where each rule is represented as:

$$IF(X_1)\ is\ (\text{In2mf1})\ AND\ (X_2)\ is\ (\text{In2mf2})\ THEN\ (Y)\ is\ (\text{Out1mf2})$$

The rules are structured as follows:

Each row represents a different fuzzy condition for input X1. Each column represents a different fuzzy condition for input X2. The intersection (table cells) represents the corresponding output fuzzy set.

For example:

The first-row states:

- If In2 is in membership function In2mf1 and In3 is in membership function In2mf1, then the output is OPT1mf1.
- If In2 is in membership function In2mf1 and In3 is in membership function In2mf2, then the output is Out1mf2.
- If In2 is in membership function In2mf1 and In3 is in membership function In3mf3, then the output is Out1mf3.

This pattern follows for the remaining rows.

The first ANFIS controller takes the direct-axis reference current $i_{d,ref}$ and actual direct-axis current $i_d$ as inputs and generates a controlled voltage to provide modified $v_{d,ref}$ . The second ANFIS controller takes $i_{q,ref} = 0$ and quadrature current $i_q$ as inputs and further refines the control process and provides modified $v_{q,ref}$ Since the $i_{q,ref} = 0$ is set to zero, this ensures that the inverter operates at a unity power factor, meaning it only delivers active power to the grid and minimizes reactive power exchange. After producing $v_{d,ref}$ and $v_{q,ref}$ , magnitude m and $\emptyset$ are calculated and fed to the sinusoidal pulse width modulation (SPWM) block to generate the switching pulses for the VSC. The current regulator gains obtained

from the ANFIS controllers are 0.3337572 and 19.1857256 respectively.

## 3.5 LCL Filter Design

For designing of LCL filter, above mentioned equations 2.14, 2.16 and 2.17 are used. After using these equations, the obtained values of LCL filter are tabulated below:

*Table 3.3: LCL Filter parameters*

| Parameters | $L_i$ (H) | $C_f$ (F) | $L_g$ (H) | $R_d$ (Ω) |
|---|---|---|---|---|
| Value | 0.2 H | 0.005 F | 0.2 | 0.1 |

## 3.6 Harmonic Distortion and FFT Analysis

Nonlinear loads cause harmonics which distort the voltage and current waveforms. Total harmonic distortion (THD) is a measure of the effective value of the harmonic voltage ($THD_v$) or current ($THD_i$) in a distorted waveform. It is the heating value of the harmonics relative to the fundamental. Low value harmonics with least probability of causing disturbing effects are present in the utility network and high value harmonics with high probability of causing disturbing effects are found in vicinity of large industries. Harmonic standards impose limits on voltage distortions which according to IEEE 519 standard given by table (2) and (3). The root mean square (rms) voltage of an ac source supplying a nonlinear load producing h harmonics is given by [14].

$$V_{rms} = \frac{1}{\sqrt{2}}\sqrt{{V_1}^2 + {V_2}^2 + .. + {V_{hmax}}^2} \quad (3.31)$$

$$= \sqrt{{V_{1,rms}}^2 + {V_{2,rms}}^2 + .. + {V_{hmax,rms}}^2} \quad (3.32)$$

$V_1$, $V_2$ …$V_h$ refer to peak magnitudes of fundamental, second and higher order current harmonics. The equivalent rms value of the current is given by,

$$I_{rms} = \frac{1}{\sqrt{2}}\sqrt{{V_1}^2 + {V_2}^2 + .. + {V_{hmax}}^2} \quad (3.33)$$

$$= \sqrt{{I_{1,rms}}^2 + {I_{2,rms}}^2 + .. + {I_{hmax,rms}}^2} \quad (3.34)$$

Total harmonic distortions (THDs) are referred to the fundamental values of voltage and currents. Voltage and current THDs are given by,

$$THD_v = \frac{1}{V_1}\sqrt{{V_{2,rms}}^2 + {V_{3,rms}}^2 + .. + {V_{hmax,rms}}^2} \quad (3.35)$$

$$THD_i = \frac{1}{I_1}\sqrt{{I_{2,rms}}^2 + {I_{3,rms}}^2 + .. + {I_{hmax,rms}}^2} \quad (3.36)$$

According to Fourier Transform theory, a continuous periodic function x(t) with a period T can be represented as a sum of sinusoidal components (fundamental and harmonics) using the Fourier Series. The Fourier series representation is given by:

$$x(t) = \sum_{n=-\infty}^{\infty} C_n e^{jnw_0 t} \quad (3.37)$$

Where, $C_n$ are the Fourier coefficients, which define the magnitude and phase of each harmonic component, $w_0 = 2\pi f_0 = \frac{2\pi}{T}$ is the fundamental angular frequency, n represents the harmonic order (integer multiples of the fundamental frequency). The Fourier Transform X(f) of x(t) gives the frequency domain representation,

$$X(f) = \int_{-\infty}^{\infty} x(t)\, e^{-j2\pi f t} dt \quad (3.38)$$

For a periodic function, the Fourier transform results in a series of impulses (Dirac delta functions) at the harmonic frequencies,

$$X(f) = \sum_{n=-\infty}^{\infty} C_n\, \delta(f - nf_0) \quad (3.39)$$

Thus, the harmonic analysis involves determining the coefficients $C_n$, which capture the magnitude and phase of each frequency component present in x(t).

In real applications, when analysing a distorted periodic waveform, the signal is first sampled at discrete time intervals before applying the Fourier Transform. The Discrete Fourier Transform (DFT) is used to analyse the fundamental and harmonic content of the sampled waveform. The Discrete Fourier Transform (DFT) is given by:

$$X(k) = \sum_{n=0}^{N-1} x(n) e^{-j\frac{2\pi}{T}kn} dt \quad (3.40)$$

n= 0,1,2……. (N-1) and N be the number of sampled points in one cycle, x(n) is the sampled time-domain signal. X(k) represents the frequency-domain components. The standard DFT has a complexity of $O(N^2)$, but the FFT reduces this to O (N log N), making it much faster, especially for large datasets. The FFT algorithm exploits the symmetry and periodicity properties of the DFT to reduce the number of required computations. The key idea is divided and conquer, where the DFT of a sequence is broken down into smaller DFTs recursively. Instead of directly computing this summation for each k, FFT algorithms- the Radix-2 Cooley-Tukey Algorithm optimize the calculations. Radix-2 Cooley-Tukey Algorithm is the most used FFT algorithm and is applicable when N is a power of 2 ($N=2^m$). It splits the DFT into two smaller DFTs: Even-indexed terms and Odd-indexed terms

Let's take x(n)= [$x_0$, $x_1$, $x_2$, $x_3$…… $x_n$] (3.41)

Even index: $[x_0, x_2 \ldots\ldots x_{2k}]$ (3.42)

Odd index: $[x_1, x_3 \ldots. x_{2k+1}]$ (3.43)

where k is a natural number.

The final FFT results for N,

$X(0) = E(0) + W_N^0 O(0)$ (3.44)

$X(1) = E(1) + W_N^1 O(1)$ (3.45)

$X(2) = E(0) - W_N^0 O(0)$ (3.46)

$X(3) = E(1) - W_N^1 O(1)$ (3.47)

and so on.

# 4. Simulations and Results

## 4.1 Simulations

### 4.1.1 Simulations of Different PV MPPT

The simulation was carried out using MATLAB/SIMULINK, and the characteristic curves along with the results were analysed for verification. A comprehensive evaluation of the topology was performed by varying circuit parameters. The selected simulation parameters include a sampling time ($T_S$) of 2 μs, a fixed step size of 1 ms, and a carrier frequency ($f_c$) of 5 kHz. The 4×10.6 KW Solar PVs are designed and simulated in MATLAB environment to supply the 9-level inverter. The PV system used for the simulation are tabulated below as in table 4.1.

*Table 4.1: Characteristics of PV*

| **Description** | **Ratings** |
|---|---|
| Nominal Power | 213.15 W |
| Maximum Power Point Voltage ($V_{MP}$) | 29 V |
| Maximum Power Point Current ($I_{MP}$) | 7.35 A |
| Open Circuit Voltage ($V_{OC}$) | 36.3 V |
| Short Circuit Current ($I_{SC}$) | 7.84 A |
| Parallel strings | 5 |
| Series Connected modules per string | 10 |

The equations 2.6 and 2.8 are used to calculate the value of L and C in order to reduce the voltage and current ripples and are obtained as L= 0.004 H and C = 0.009 F.

The algorithm is implemented as an embedded function on MATLAB/Simulink. The inputs of the algorithm are $V_{oc}$, $I_{sc}$ and T. Two pilot cells are used and $V_{oc}$ and $I_{sc}$ are obtained using these two pilot cells. This algorithm was found to track the MPP even with rapid variation of climatic conditions. As shown in Figure 4.1, the system output varies between 0.25 and 0.75, failing to reach the Maximum Power Point (MPP). Furthermore, it experiences steady-state oscillations and a prolonged convergence time

ranging from 0.75 to 1. As a result, the metric analysis demonstrates that the model has a very low efficiency. This type of evaluation can be applied to all MPPT models. To test the algorithm an irradiation model as shown in figure 4.1 is applied to the Simulink model shown in figures 4.2, 4.3 and 4.4.

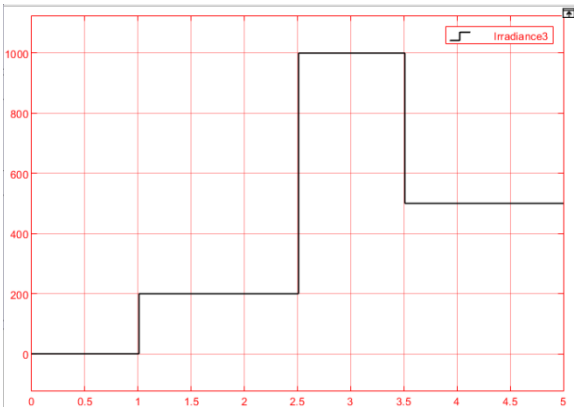


Fig. 4.1. Irradiation Model Applied to Simulink Model

For the comparative study purpose, the Simulink model of a Perturb and Observe, Incremental Conductance and GA based MPPT algorithm was developed as shown in figures 4.2, 4.3, 4.4. The algorithm has been tested extensively using simulation software.

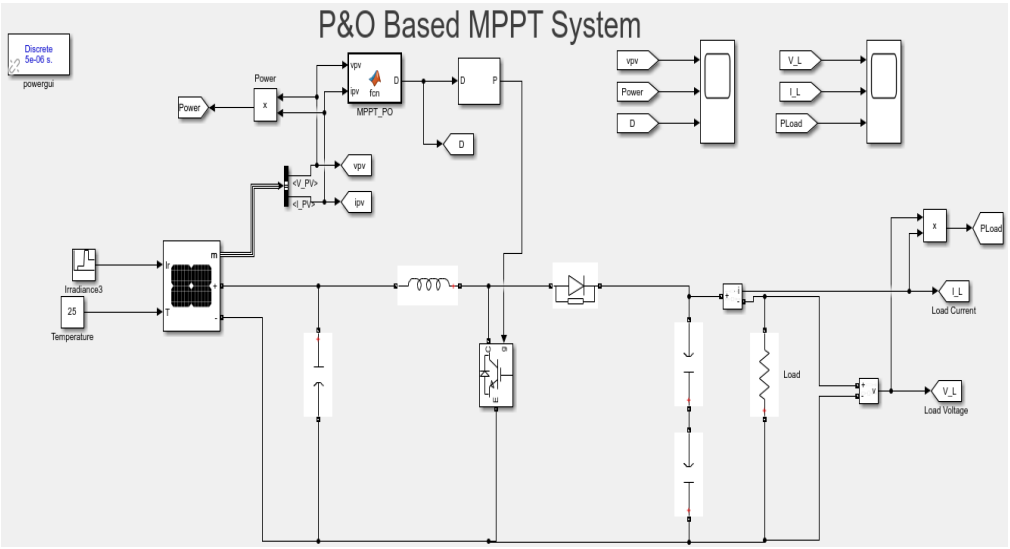


Fig. 4.2. Simulink Model for P&O algorithm Based PV system

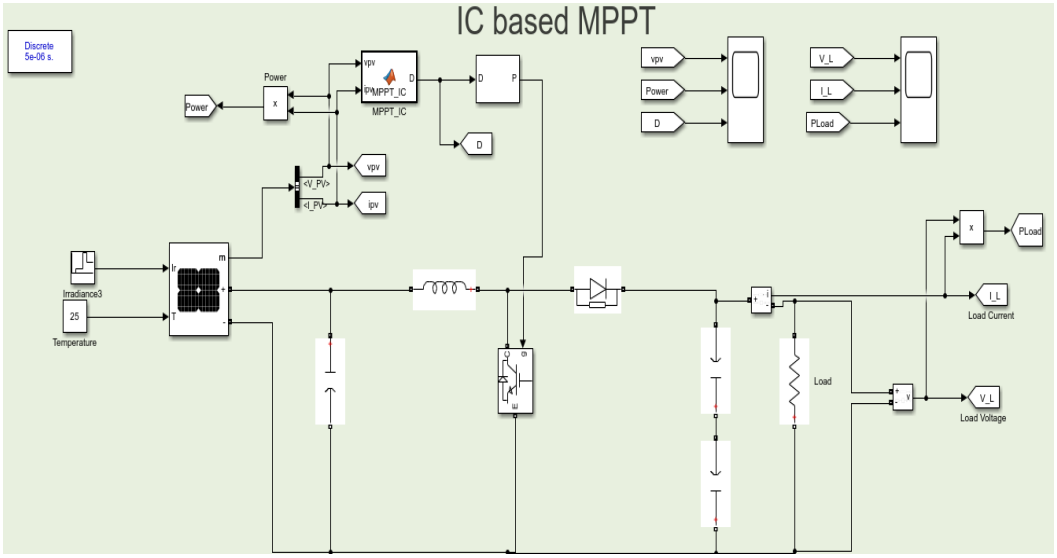


Fig. 4.3. Simulink Model for INC algorithm Based PV system

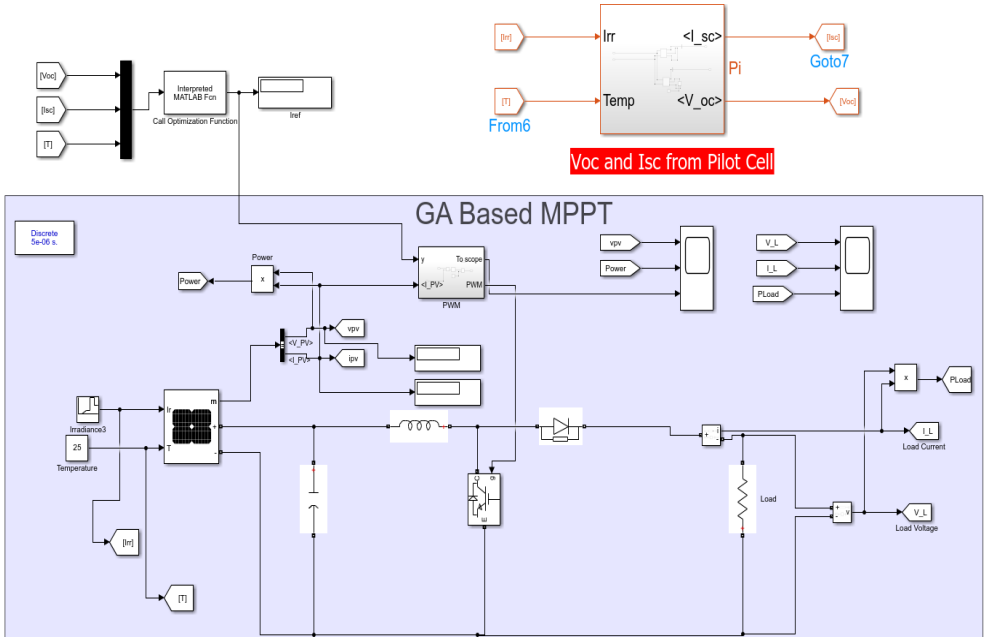


Fig. 4.4. Simulink Model for GAs Based PV system

The CFFNN is trained using more than 20,000 data points including input and output functions for varying irradiances and temperature conditions., ensuring that model can generalize well under different scenarios during partial shading conditions and non- linearities presented in the system. The simulation model as in figure 4.5 undergoes 2000+ epochs during model trainings. The gradient descent method is used for optimization of weightage and mean squared error loss function for minimizing the errors. The training loss is reduced to $1.203 \times 10^{-20}$. The validation is performed by μ (adaptive learning rate) and gradient are analysed for stability.

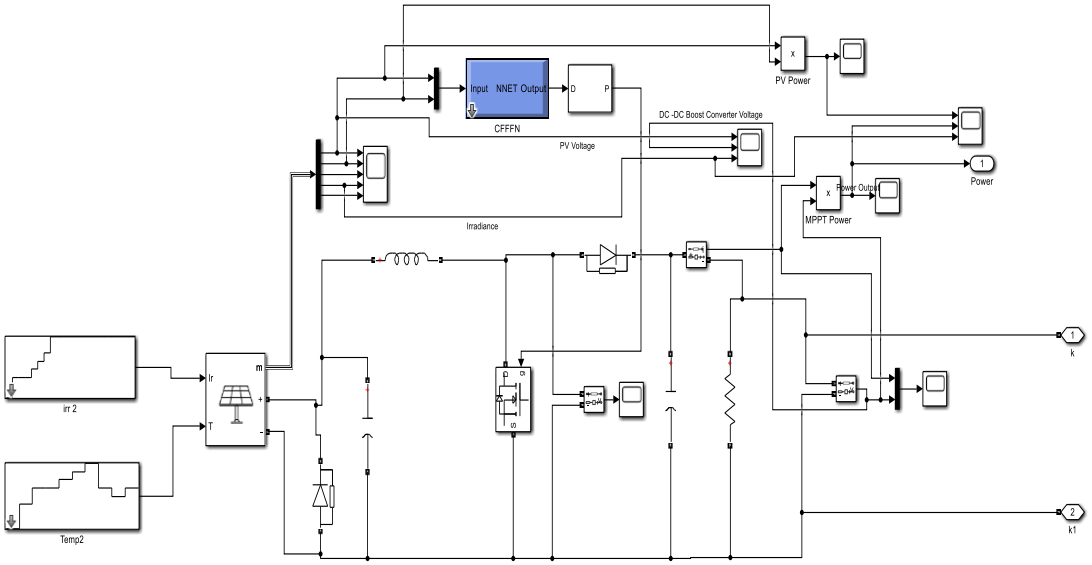


Fig. 4.5. Simulink Model for CFFNN Based PV MPPT system

The duty obtained from the simulation in the MATLAB Simulink as 0.3074.

This confirms that the high accuracy of CFFNN- based MPPT algorithm for PV system under various environmental conditions. The advantages of CFNN for MPPT are: Captures Nonlinearities, Faster Convergence, Higher Accuracy, Robust to Noise, Improved Generalization. The six hidden layered CFFNN structure is as shown in figure 4.6.

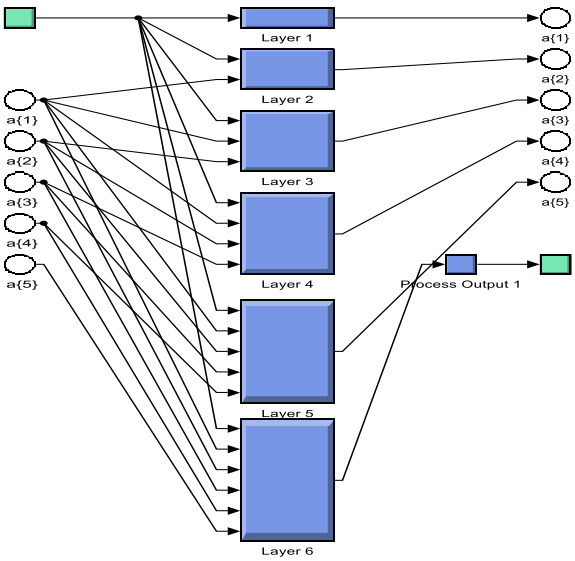


Fig. 4.6. CFFNN Hidden Layers

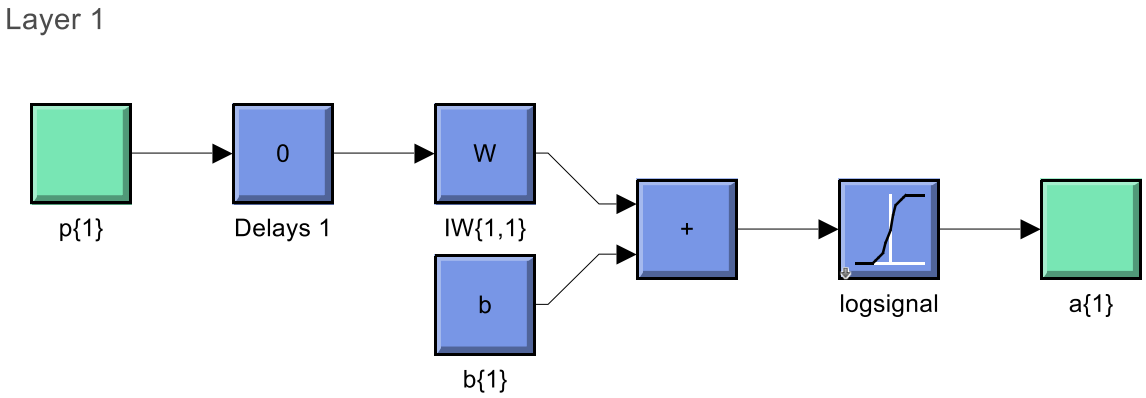


Fig. 4.7. CFFNN Layer 1

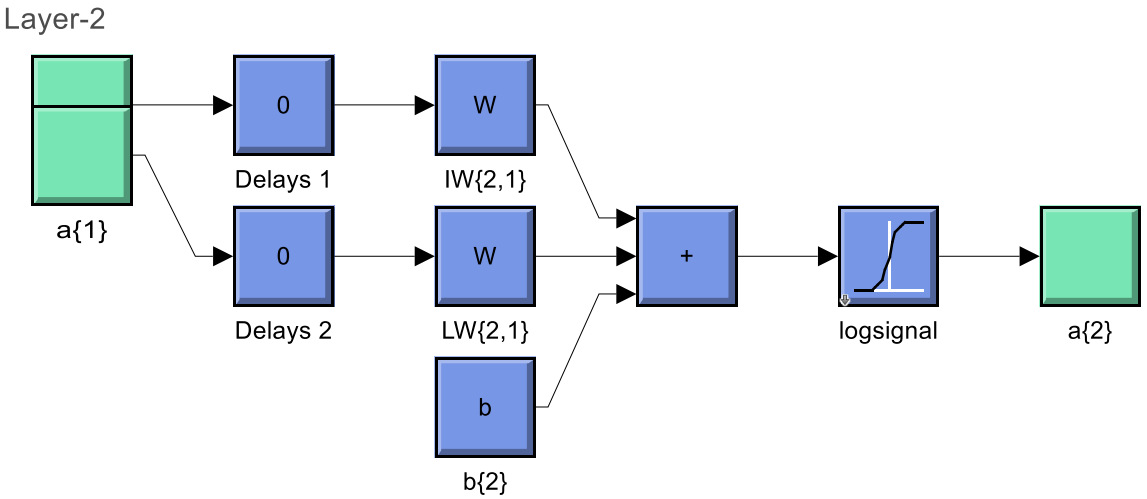


Fig. 4.8. CFFNN Layer 2

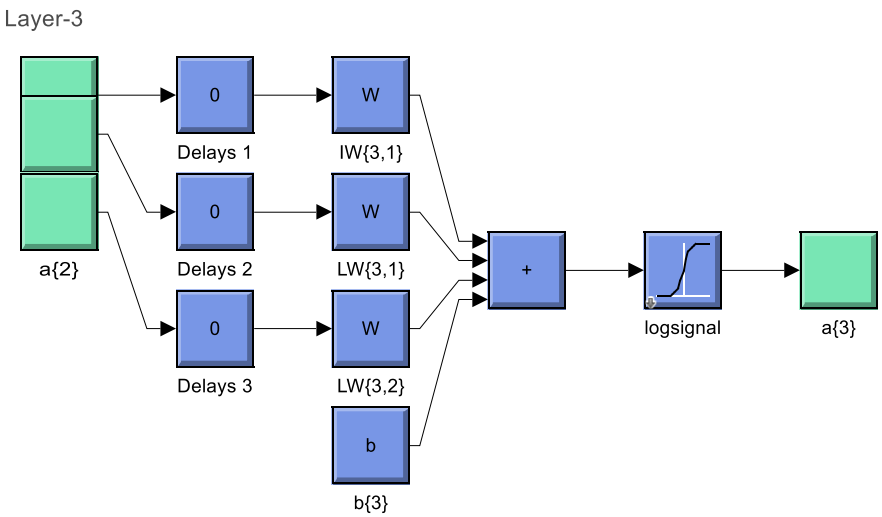


Fig. 4.9. CFFNN Layer 3

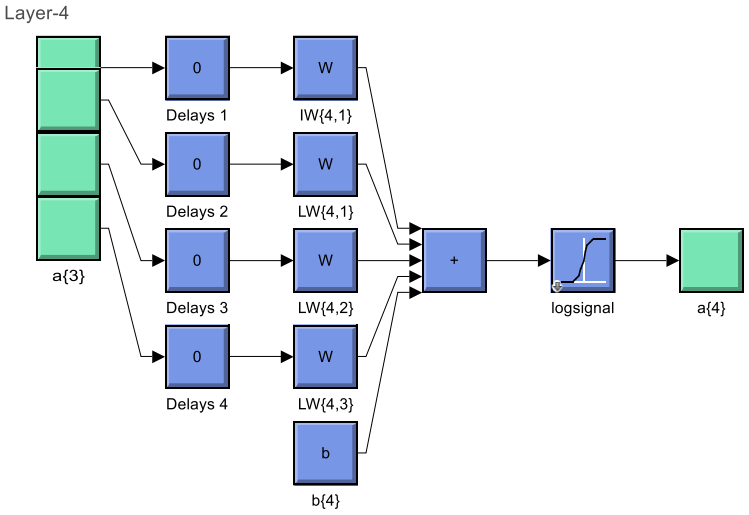


Fig. 4.10. CFFNN Layer 4

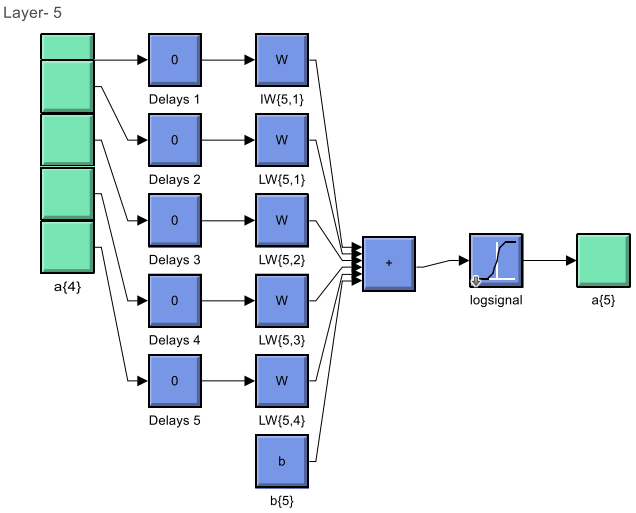


Fig. 4.11. CFFNN Layer 5

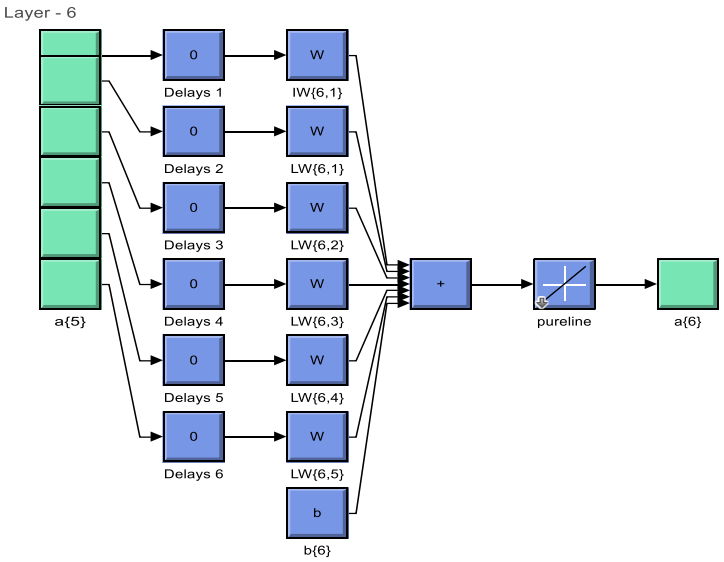


Fig. 4.12. CFFNN Layer 6

### 4.1.2 Simulations of 9- Level Inverter

The simulations diagram for the 9- level inverter is as shown in figure 4.13 below.

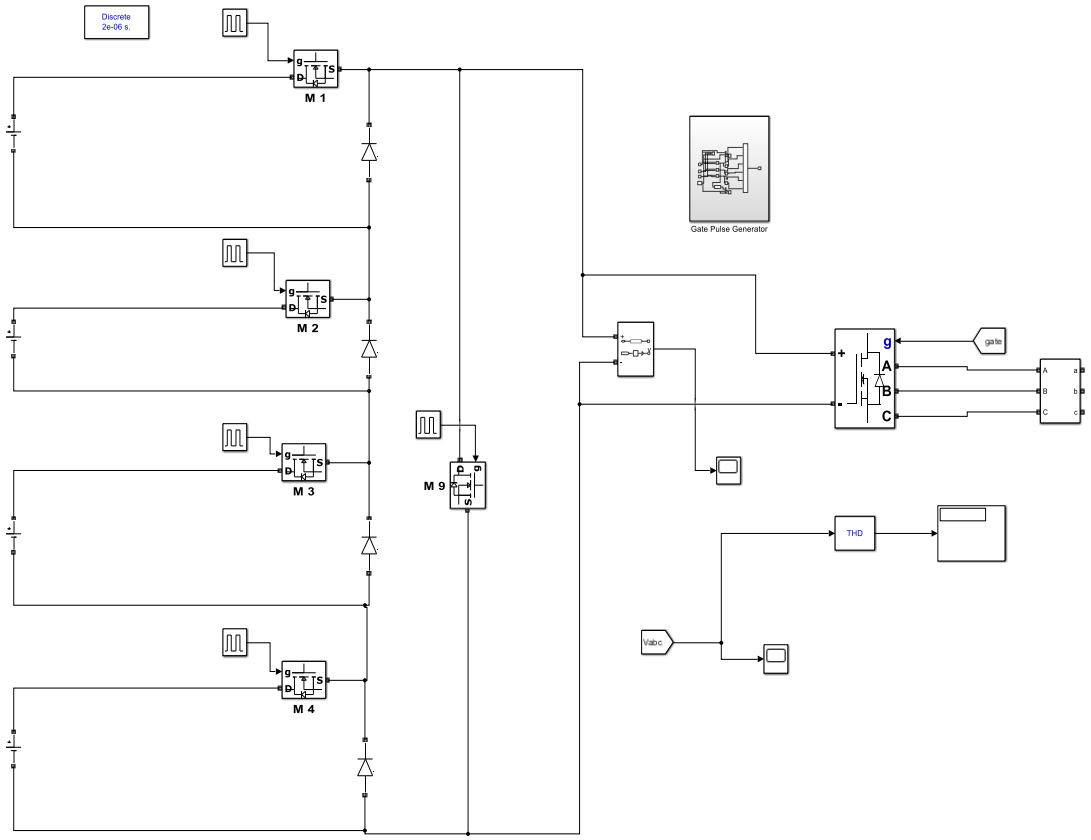


Fig. 4.13. Simulink Model of Nine- Level Inverter

### 4.1.3 Simulations of Main VSC Controller

The characteristics of main VSC controller is tabulated as in table 4.2.

*Table 4.2: Characteristics of Main VSC*

| Characteristics | Values |
|---|---|
| Nominal power $P_{nom}$ | 100 KVA |
| Nominal frequency $f_{nom}$ | 50 Hz |
| Nominal DC bus voltage ($V_{DC}$) | 700 V |
| DC Voltage regulator gains ($K_p$, $K_i$) | 10.0031579, 812.235575 |
| Current regulator gains ($K_p$ $K_i$) | 0.3337572 ,19.1857256 |
| Nominal rms voltages ($V_{rms-LL}$) | 380 V |
| Switching frequency | 5 KHz |

The simulation of voltage source converter control mechanism for current regulator is as shown in figure 4.14.

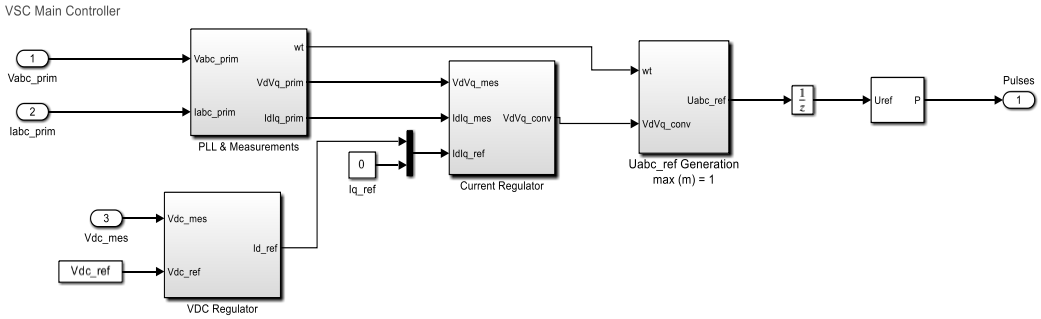


Fig. 4.14. Simulink Model of VSC Main Controller

### 4.1.4 Simulations of 9 level Inverter with PV MPPT

The simulation of 9 level inverter with PV system is as shown in figure 4.15.

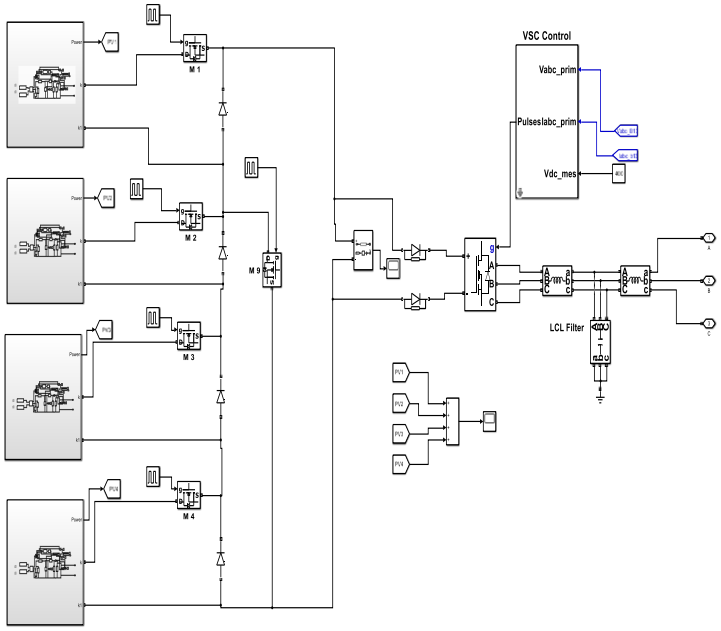


Fig. 4.15. Simulink Model of Overall System

### 4.1.5 Simulation of ANFIS Based GC Inverter with CFFNN PV MPPT

The simulation of ANFIS based grid connected inverter with CFFNN PV MPPT system along with the distribution load is as shown in figure 4.16.

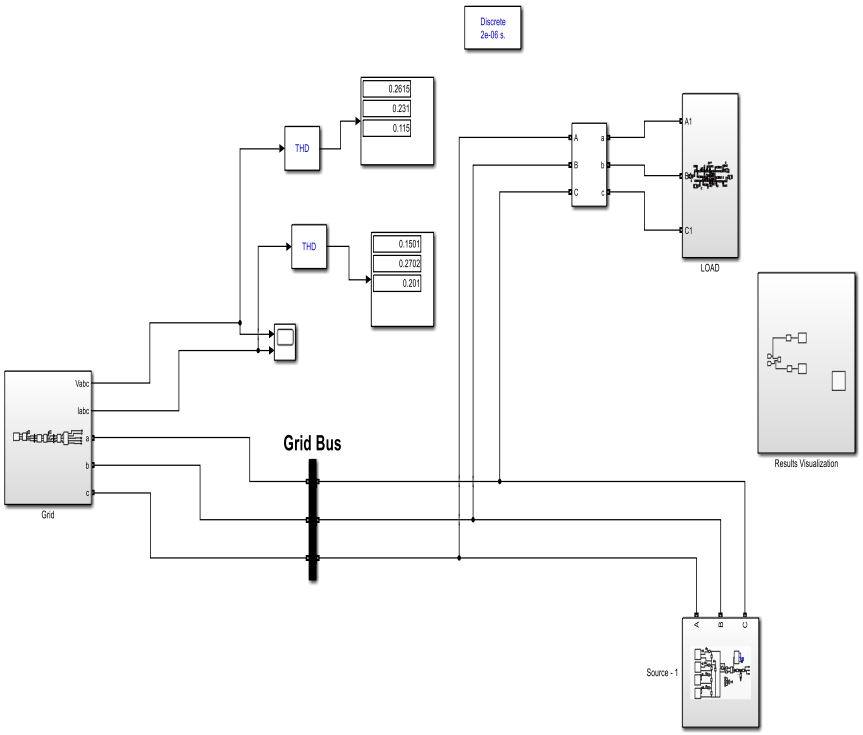


Fig. 4.16. Simulink Model of GC PV system with 19 Bus DS

The distribution load test model consisting of linear as well as non-linear loads implemented in the figure 4.17 is as shown in figure.

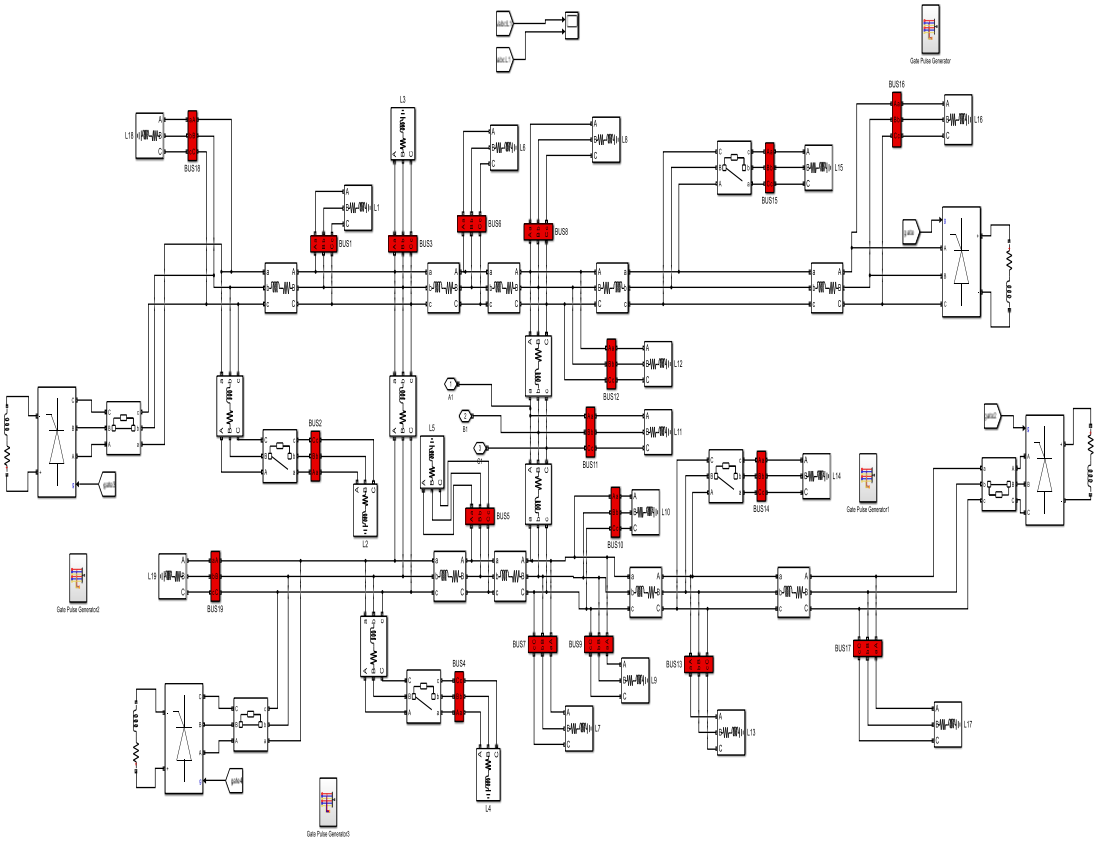

Fig. 4.17. Load Test Distribution model

### 4.1.6 Simulations of ANFIS Based Controller

The simulation of ANFIS based controller for main VSC control is as shown in figure 4.18. Figures show the hidden layer of ANFIS controller.

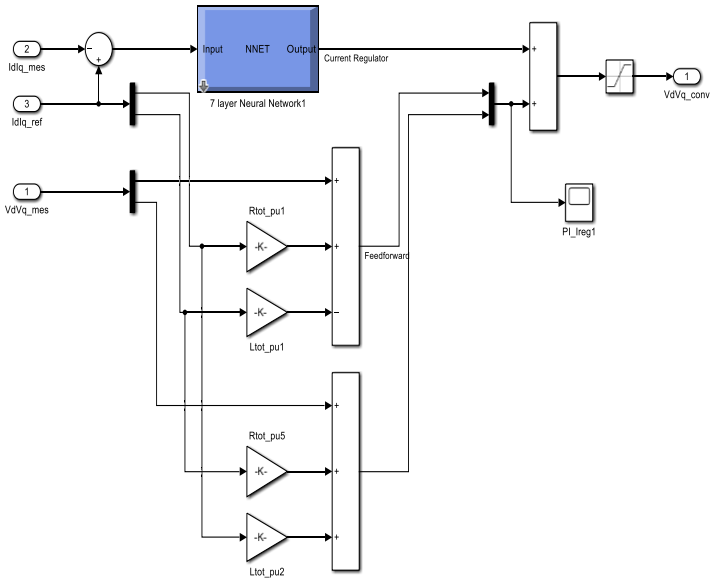


Fig. 4.18. ANFIS Based Current Regulator

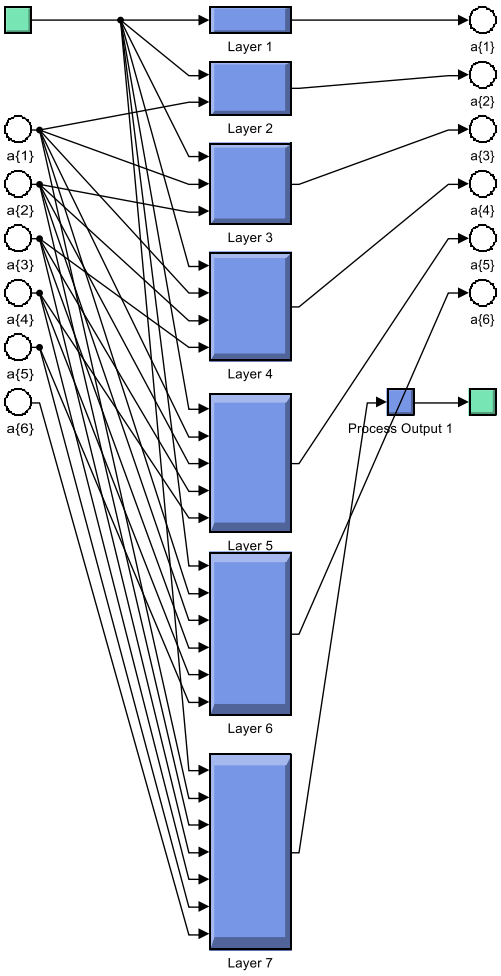


Fig. 4.19. Hidden Layer of ANFIS Based Controller

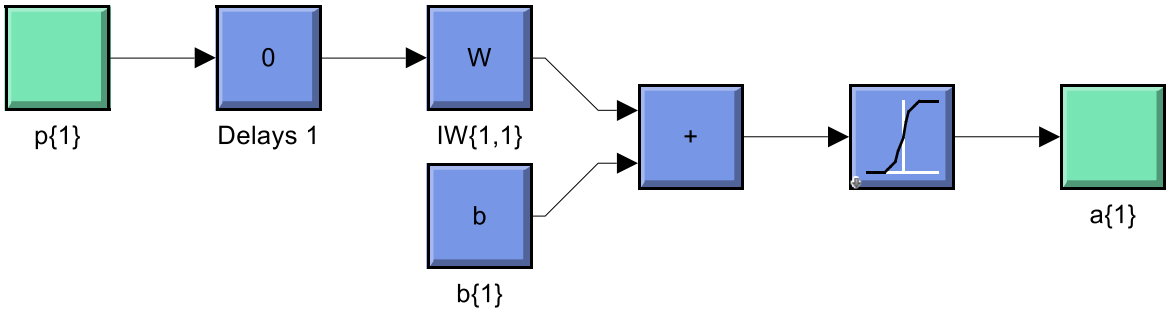


Fig. 4.20. ANFIS Hidden Layer – 1

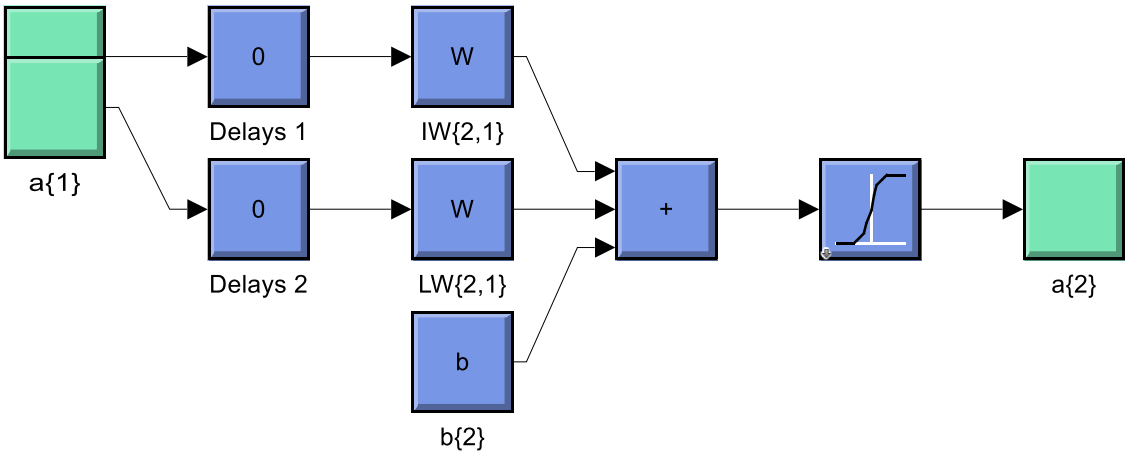


Fig. 4.21. ANFIS Hidden Layer – 2

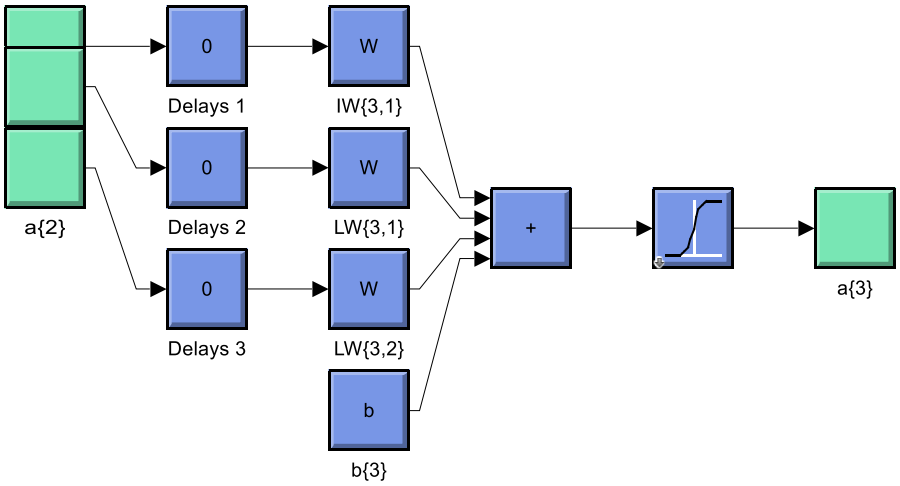


Fig. 4.22. ANFIS Hidden Layer – 3

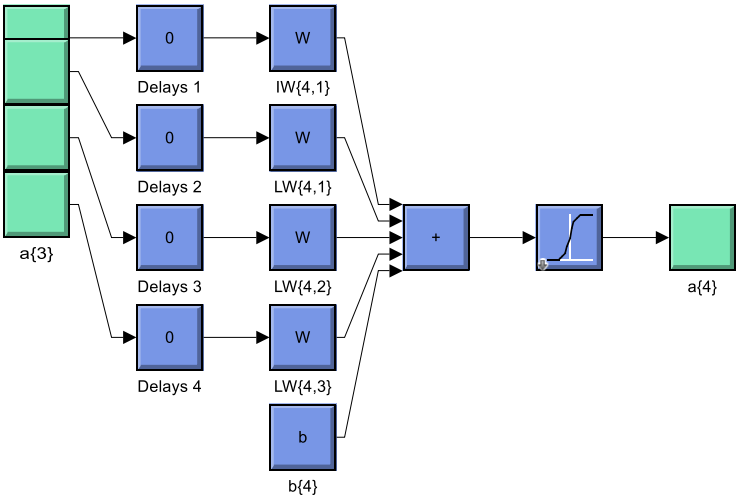


Fig. 4.23. Hidden Layer – 4

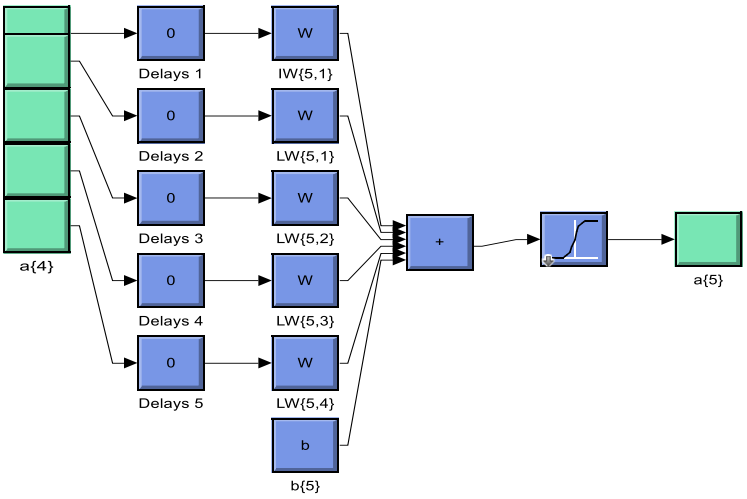


Fig. 4.24. ANFIS Hidden Layer – 5

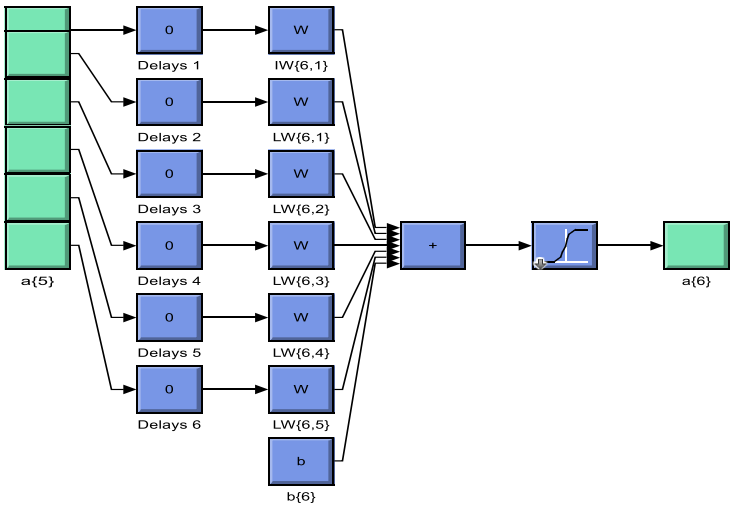


Fig. 4.25. ANFIS Hidden Layer – 6

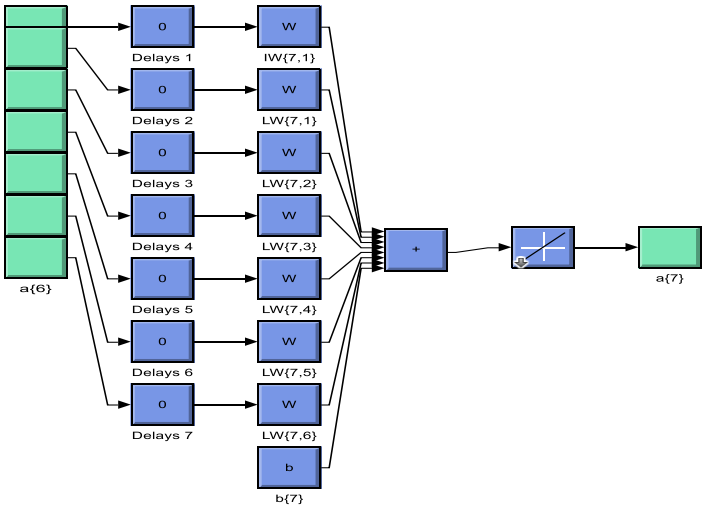


Fig. 4.26. ANFIS Hidden Layer – 7

## 4.2 Results

### 4.2.1 Results of Different MPPT Techniques

In figure 4.27 initially, the voltage VPV remains near 0V until about 1 second, then increases sharply to approximately 14V with some oscillations. Around 2.5 seconds, it spikes to about 35V before stabilizing at roughly 30V after 2.8 seconds. The power output remains at 0W until around 1 second, when it sharply increases to about 45W. After some fluctuations due to the PO's fine-tuning of the Maximum Power Point (MPP), the power stabilizes around 100W from 2.7 seconds onwards, indicating the system is operating effectively at or near its maximum power.

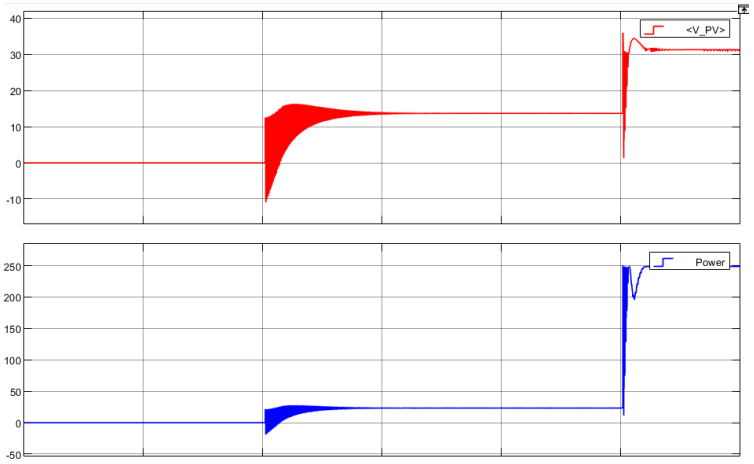


Fig. 4.27. Evolution of power and voltage using P&O

In figure 4.28 initially, the voltage $V_{PV}$ remains near 0V until about 1 second, then increases sharply to approximately 22V with some oscillations. Around 2.5 seconds, it spikes to about 35V before stabilizing at roughly 30V after 3.5 seconds. The power output remains at 0W until around 1 second, when it sharply increases to about 45W. After some fluctuations due to the IC's fine-tuning of the Maximum Power Point (MPP), the power stabilizes around 100W from 3.5 seconds onwards, indicating the system is operating effectively at or near its maximum power.

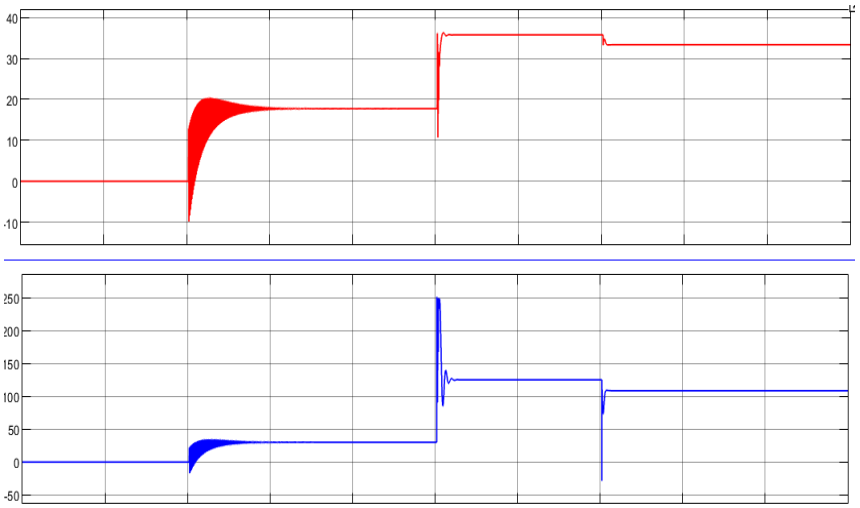


Fig. 4.28. Evolution of power and voltage using INC

In figure 4.29 initially, the voltage $V_{PV}$ remains near 0V until about 1 second, then increases sharply to approximately 15V with less oscillations. Around 2.5 seconds, it spikes to about 32V before stabilizing at roughly 30V after 2.6 seconds. The power output remains at 0W until around 1 second, when it sharply increases to about 45W. After some fluctuations due to the GA's fine-tuning of the Maximum Power Point (MPP), the power stabilizes around 100W from 2.5 seconds onwards, indicating the system is operating effectively at or near its maximum power.

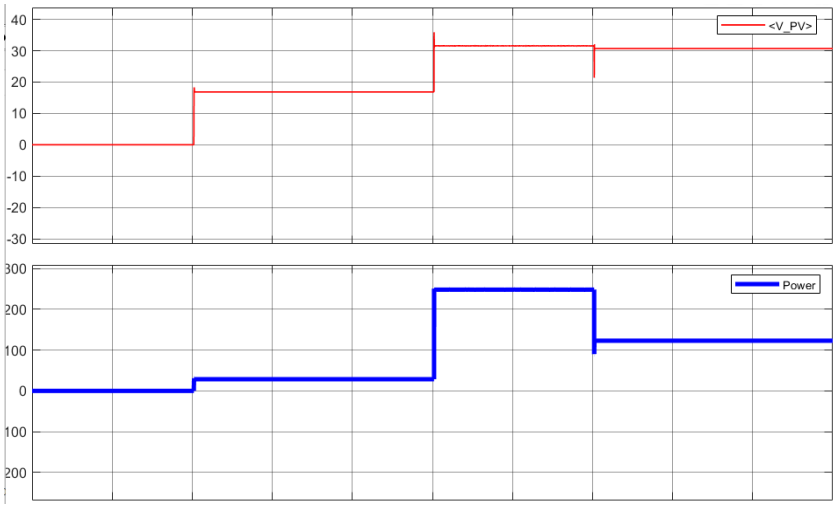


Fig. 4.29. Evolution of power and voltage using GA

The output power and output voltage obtained from the solar PV by using CFFNN MPPT is as shown in figure 4.30 and 4.31 respectively. We can see that, the oscillations in the output power and voltage of output of boost converters are reduced so that it can enhance the stability, efficiency and can provide the fast convergence time.

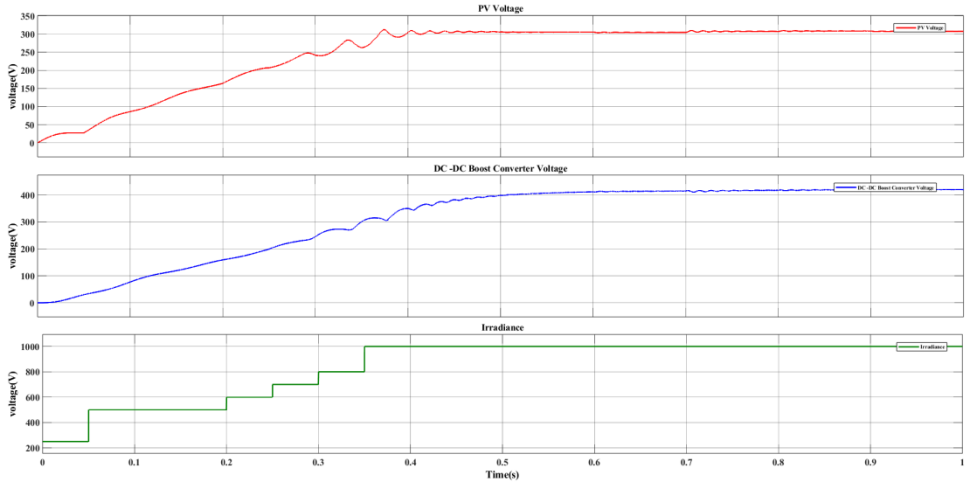


Fig. 4.30. Panel's Output Voltage, MPPT's Output Voltage and Irradiance

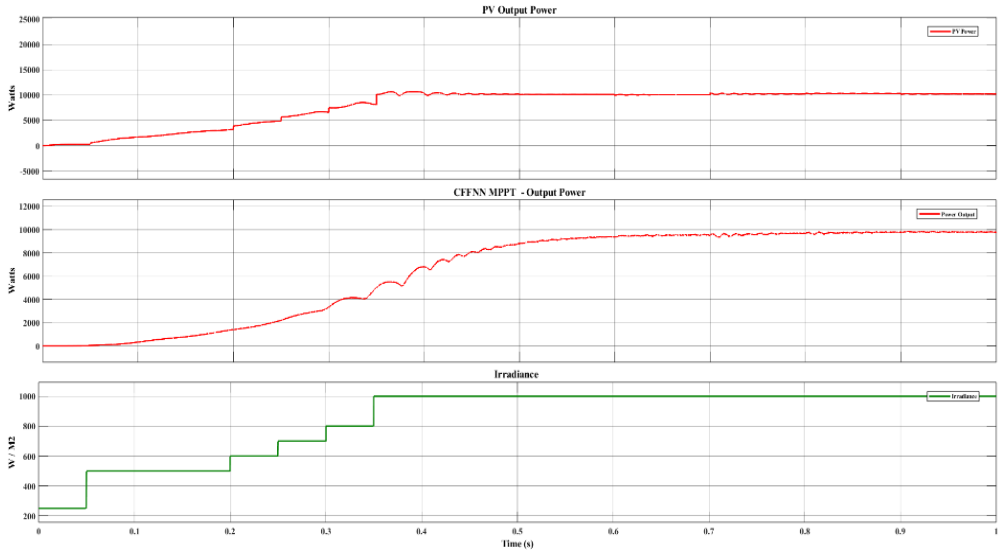


Fig. 4.31. Output Power with CFFNN MPPT

The output voltage for the nine-level cascaded H- bridge inverter with reduced harmonics is as shown in figure 4.32. This 9 – level inverter can reduce the harmonics contents in the output voltage so that it can help to enhance the power quality issues for all types of loads.

### 4.2.2 Results of MLI

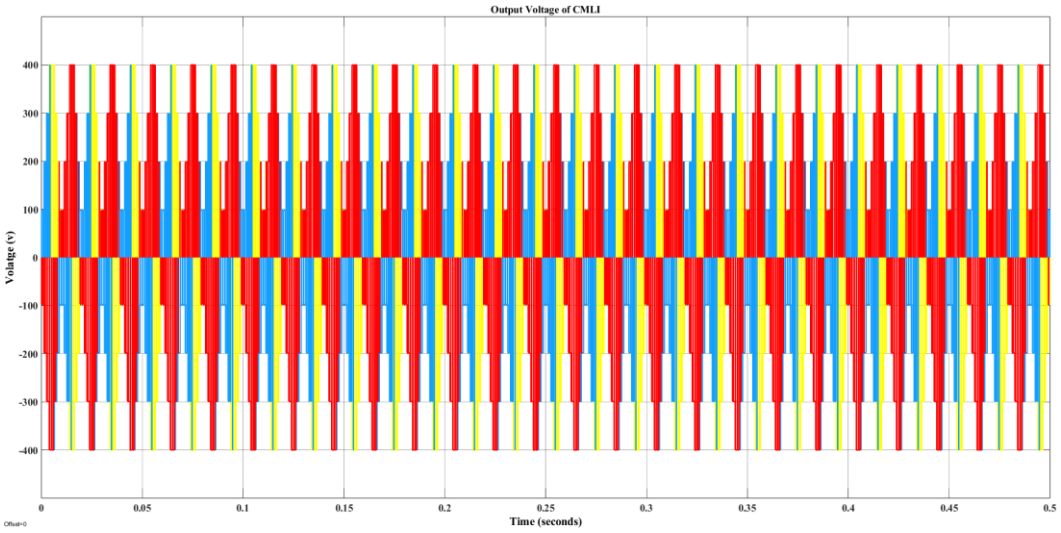


Fig. 4.32. Output voltage of 9- level Inverter

The distribution test model for the testing is shown in Figure 4.33, it consists of 19 different load buses in which different types for loads are tapped. There are various switching loads which are switching for the certain instants (0.1 to 0.5 s, 0.1 to 0.3 s, 0.1 to 0.9s respectively at different buses). Due to these switching loads, there is the occurrence of PQ issues. By implementing the ANFIS controller based 9- level inverter, the harmonics contents in the output voltage and currents are reduces as shown in figure 4.34 and 4.35. The distribution bus model consisting of switching of linear as well as non-linear loads consequently the power quality issues occur in the load's voltage and current. The distribution load test model is simulated and validated in the MATLAB Simulink to analyze the harmonics contents in the different buses.

### 4.2.3 Results of Output Voltage, Current and THD Analysis

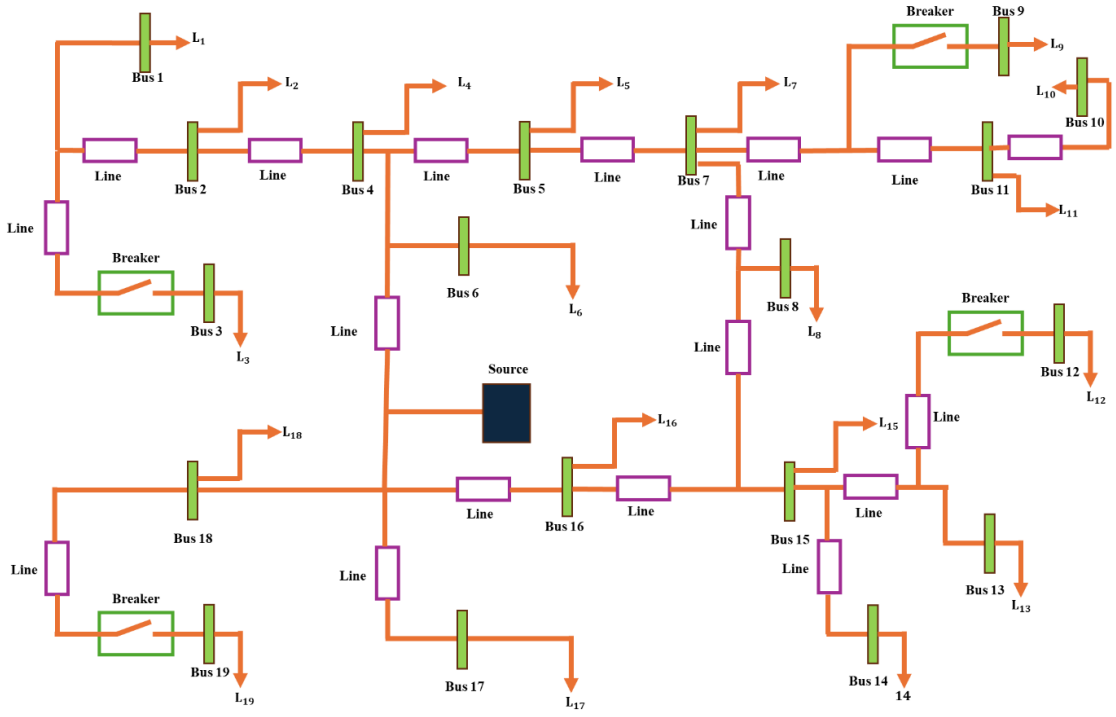


Fig. 4.33. SLD of Simulation Distribution Loads Test Model

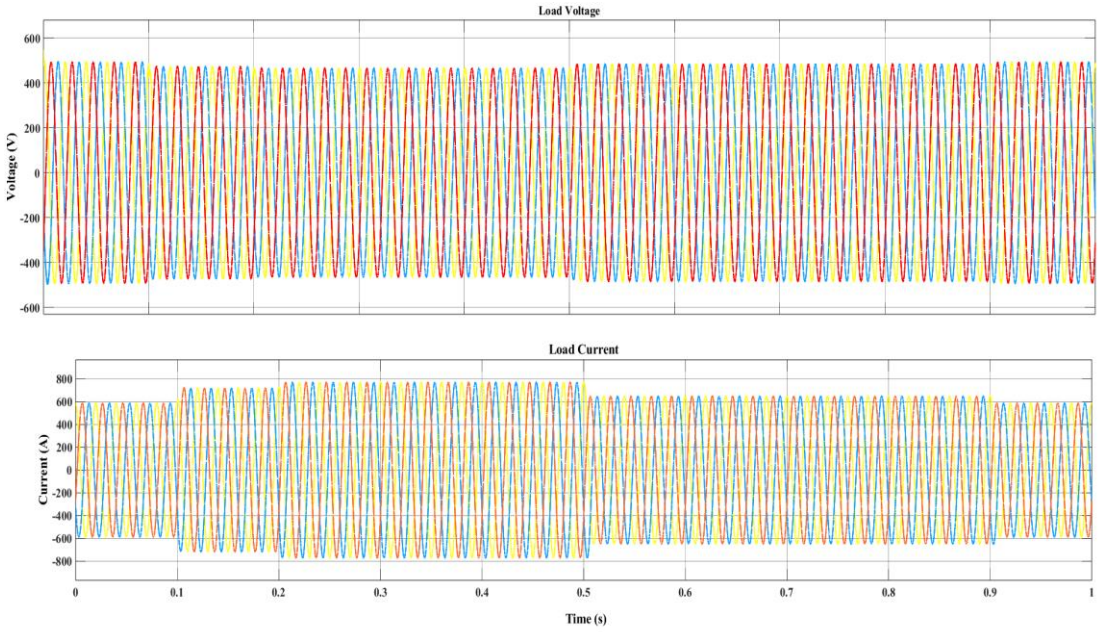


Fig. 4.34. Load Voltage and Current waveforms

The output voltage and current waveforms shows that there is some sag in the output voltage if the nonlinear loads are switched at the instant of 0.1 s and this can lead to the power quality issues in the output voltage and current. Clearly, we can see that the addition of loads at 0.1 s. But by implementing the 9 level ANFIS based inverter,

harmonics present in the output voltage and current are reduces within the IEEE 519 standard limit as mentioned in table 2 and 3. The THDs in the output voltage and currents are 0.30% and 0.01 % respectively as shown in figure 4.36 and 4.37 respectively.

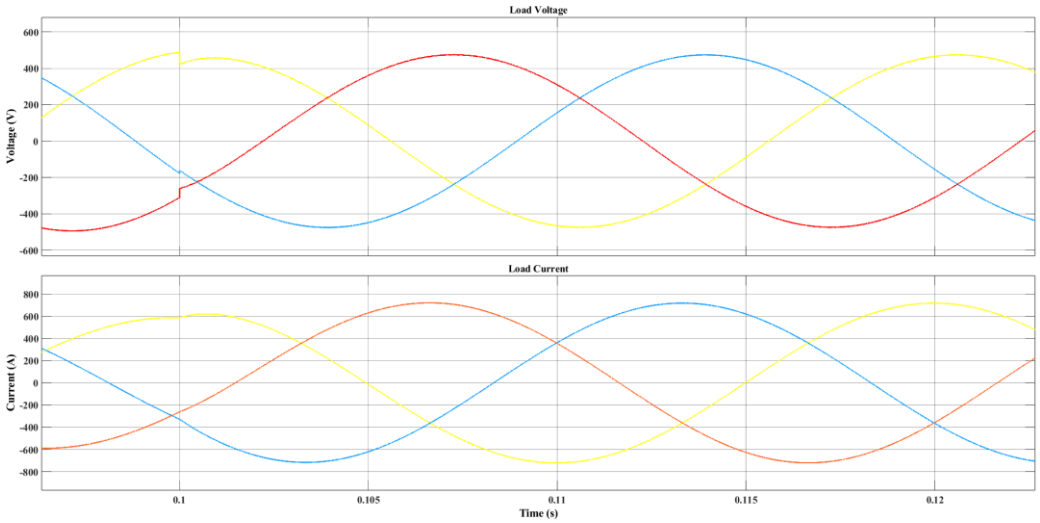


Fig. 4.35. Zoom View for switching instants and improvement in PQ

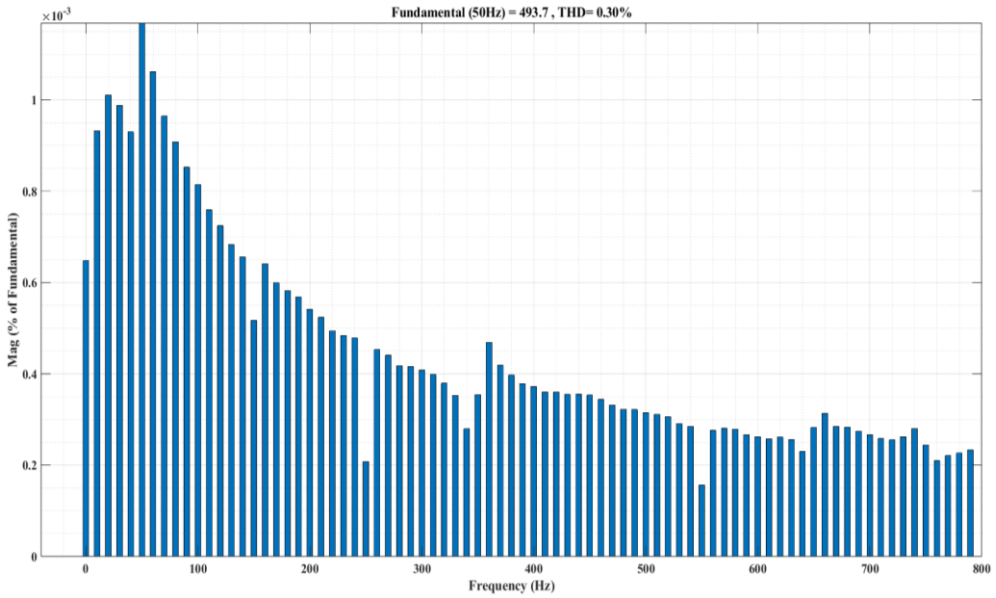


Fig. 4.36. THD in Load Voltage

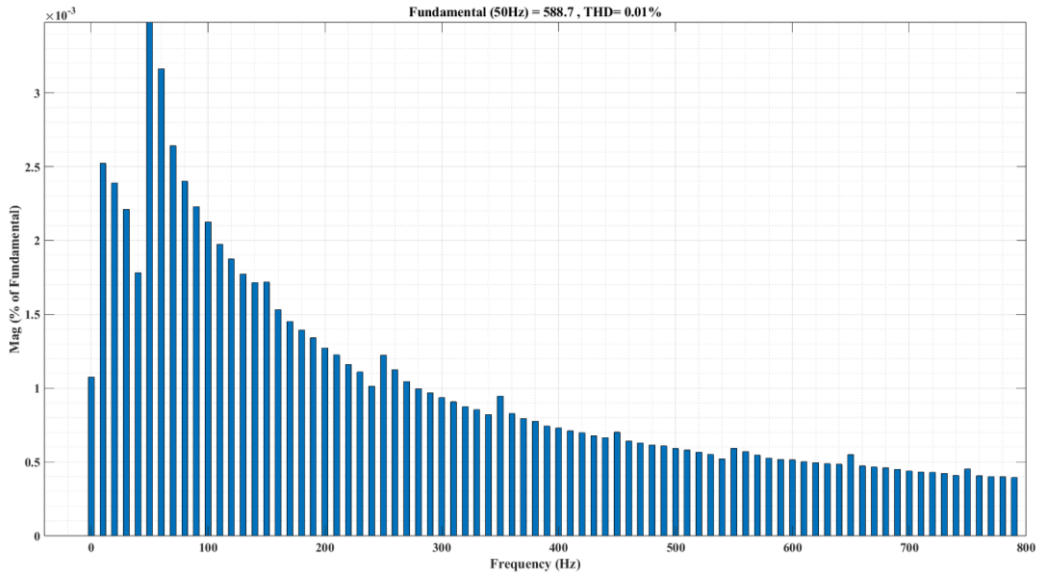


Fig. 4.37. THD in Load Current

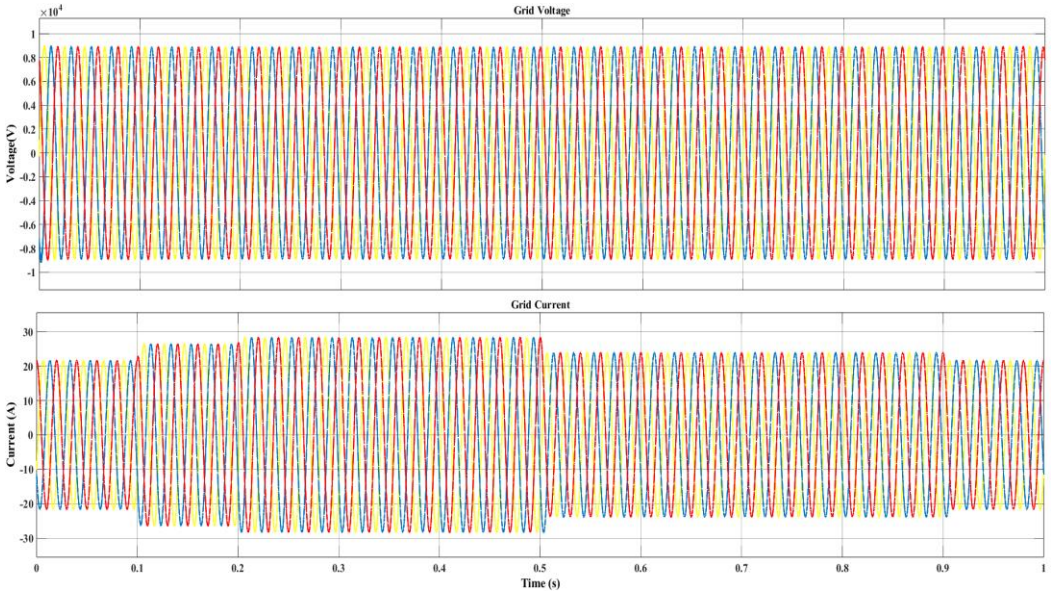


Fig. 4.38. Grid Voltage and Current waveforms

The THDs in the output voltage and currents are 0.31% and 0.01 % respectively as shown in figure 4.39 and 4.40 respectively.

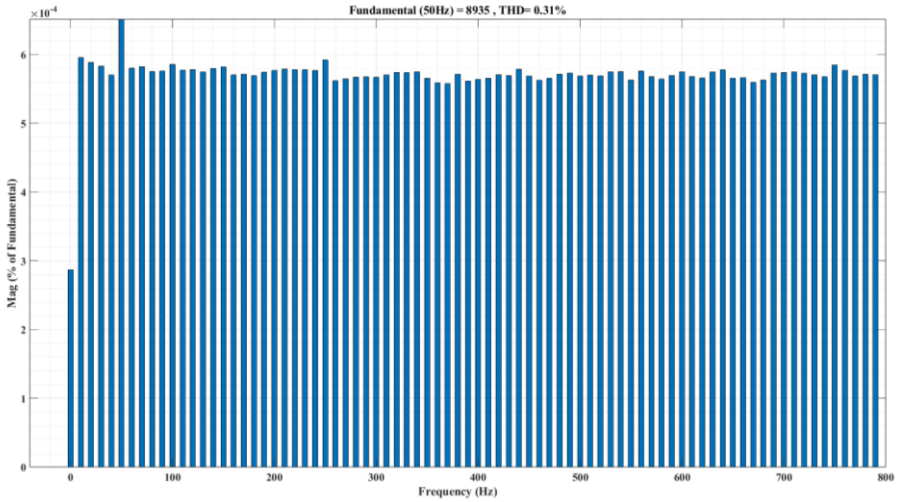


Fig. 4.39. THD in Grid Voltage

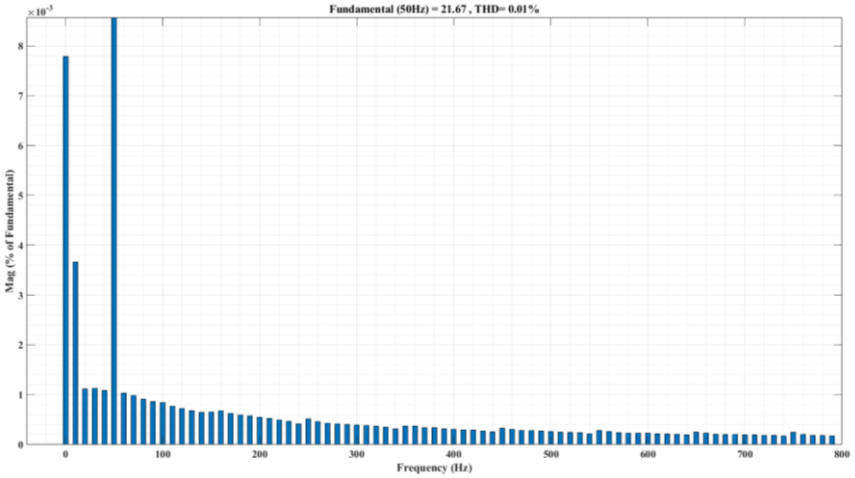


Fig. 4.40. THD in Grid Current

The THDs are also observed at different load buses. The THDs getting at different load buses are as tabulated in table 4.3.

*Table 4.3: THDs in Voltage and Currents of Load buses*

| Bus no. | 1 | 2 | 3 | 4 | 5 | 6 | 7 | 8 | 9 | 10 |
|---|---|---|---|---|---|---|---|---|---|---|
| THD in Voltage (%) | 0.17 | 4.21 | 1.63 | 4.35 | 2.04 | 1.08 | 1.86 | 0.71 | 1.86 | 1.86 |
| THD in Current (%) | 0.01 | 6.51 | 1.75 | 6.43 | 1.46 | 1.39 | 1.21 | 0.93 | 1.21 | 1.30 |

| Bus no. | 11 | 12 | 13 | 14 | 15 | 16 | 17 | 18 | 19 |
|---|---|---|---|---|---|---|---|---|---|
| THD in Voltage (%) | 0.74 | 0.71 | 3.55 | 0.41 | 0.28 | 2.88 | 0.15 | 0.21 | 0.21 |
| THD in Current (%) | 0.84 | 0.95 | 1.91 | 2.30 | 2.19 | 1.19 | 0.23 | 0.45 | 0.35 |

The THDs present at each bus are within the limit described in the table 2 and 3.

# 5. CONCLUSION AND FUTURE ENHANCEMENT

## 5.1 Conclusion

Firstly, this thesis presents a novel and effective GA-based MPPT method that demonstrates superior speed and stability in generating PV power output. The approach addresses power oscillations around the MPP and improves the applicability of linear MPPT methods, showing promise for tracking MPP in complex conditions by finding global optima.

Secondly, a ML based three -phase nine-level PWM inverter has been simulated for a grid-connected PV system to improve the power quality problems. The modulation and control of this multilevel inverter (MLI) topology are based on a ANFIS current controller based PWM technique. The inverter is integrated with a PV system and synchronized with the utility grid. The DC link voltage of each inverter module is boosted to the required level using a conventional boost converter, which derives its duty cycle from the MPPT algorithm. The CFFNN based MPPT algorithm has been employed to ensure maximum power extraction from the solar PV array. The system is designed to transfer solar energy efficiently into a three-phase utility grid and linear as well as nonlinear loads switching at different instants. The inverter's output voltage and frequency are regulated to match the grid parameters, ensuring that the power factor remains unity (UPF). A ANFIS current control algorithm has been implemented to maintain sinusoidal grid current while achieving a fast dynamic response under varying irradiances and temperature conditions. The current regulator parameters have been optimized to ensure effective grid synchronization and minimal harmonic distortion. Finally, the THDs are analysed using FFT technique. The THDs in load’s terminal (output) voltage and current are 0.30% and 0.31 % respectively. Also, the THDs in grid’s voltage and current are 0.31% and 0.01% respectively which are verified that the harmonics contents in the output voltage and currents are within the IEEE 519 standard limit. The simulation results have been validated against theoretical predictions, demonstrating successful operation. Based on these findings, the system is considered suitable for experimental implementation.

## 5.2 Limitations

While the thesis presents a GA-based MPPT method and a ML-based nine-level PWM inverter for a grid-connected PV system, there are certain limitations and challenges that must be considered.

- Implementing the ANFIS-based current controller in a real-time DSP or FPGA environment might introduce sampling and processing delays, affecting performance.
- The system performance under weak grid conditions or low short-circuit ratio (SCR) scenarios is not addressed.
- ANFIS current control requires training datasets, and performance might degrade under unknown disturbances or sudden grid faults.
- The thesis does not cover fault ride-through (FRT) capability, which is crucial for grid-connected PV inverters.
- The GA-based MPPT may struggle with fast-changing irradiance conditions due to its iterative nature.

## 5.3 Future Enhancement

The thesis work will suggest for the following future works:

- Implement fault ride-through (FRT) capability to ensure compliance with modern grid codes.
- Investigate the inverter's performance during grid disturbances such as: Voltage sags and swells, frequency deviations, grid faults.
- Develop a control mechanism to adjust inverter operation under low short-circuit ratio (SCR) conditions.
- Investigate soft-switching techniques (ZVS/ZCS) to reduce switching losses.
- The system can be extended to include energy storage (batteries or supercapacitors) for peak load management, grid support during outages, smoother power injection during transients.
- Explore Hybrid MLIs that combine Cascaded H-Bridge (CHB) and Neutral Point Clamped (NPC) topologies.

# REFERENCES


[1] M. B. Marzuki, R. T. Naayagi and V. Phan, "Modelling and simulation of Multilevel Inverter for grid connected Photovoltaic system", *2016 IEEE Region 10 Conference (TENCON)*, 2016.

[2] N. Pandiarajan and R. Muthu, "Viability analysis on photovoltaic configurations", *Proceedings of the IEEE Region 10 Conference (TENCON '08)*, November 2008.

[3] S. Singh, S. Manna, M. I. Hasan, Mansoori and A. K. Akella, "Implementation of Perturb & Observe MPPT Technique using Boost converter in PV System", *2020 International Conference on Computational Intelligence for Smart Power System and Sustainable Energy (CISPSSE)*, pp. 1-4, 2020.

[4] S. J. Park, F. S. Kang, M. H. Lee and C. U. Kim, "A new singlephase five level PWM inverter employing a deadbeat control scheme", *IEEE Trans. Power Electron*, vol. 1, no. 18, pp. 831-843, May 2003.

[5] L. M. Tolbert and T. G. Habetler, "Novel multilevel inverter carrierbased PWM method", *IEEE Trans. Ind. Appl*, vol. 35, no. 5, pp. 1098-1107, SepJOct. 1999.

[6] S. A. Arefifar and Y. A.-R. I. Mohamed, "Probabilistic optimal reactive power planning in distribution systems with renewable resources in grid-connected and islanded modes," *IEEE Trans. Ind. Electron.*, vol. 61, no. 11, pp. 5830-5839, Nov. 2014.

[7] G. Heydt, *Electric Power Quality*, Stars in a Circle Publications, Dec. 1991.

[8] Y. Onal, "A New Controller for Photovoltaic Panel Fed Unified Power Quality Conditioner to Power Quality Improvement," *Mugla Journal of Science and Technology*, vol. 7, no. 1, pp. 14-24, 2021.

[9] E. Hossain, M. R. Tür, S. Padmanaban, S. Ay, and I. Khan, "Analysis and Mitigation of Power Quality Issues in Distributed Generation Systems Using Custom Power Devices," *IEEE Access*, vol. 6, pp. 16816-16833, 2018.

[10] Y. Han, Y. Feng, P. Yang, L. Xu, Y. Xu, and F. Blaabjerg, "Cause, Classification of Voltage Sag, and Voltage Sag Emulators and Applications: A Comprehensive Overview," *IEEE Access*, vol. 8, pp. 1922-1934, 2020.

[11] R. Langella, A. Testa, and et al., "IEEE Recommended Practice and Requirements for Harmonic Control in Electric Power Systems," *IEEE*

*Recommended Practice*, IEEE, 2014.

[12] H. D. Liu, C. H. Lin, K. J. Pai, and Y. L. Lin, "A novel photovoltaic system control strategy for improving hill climbing algorithm efficiencies considering radiance and load effects," *Energy Convers. Manag.*, vol. 165, pp. 815–826, 2018.

[13] R. Alik, A. Jusoh, and T. Sutikno, "A review on perturb and observe maximum power point tracking in photovoltaic systems," *Telecommun. Comput. Electron. Control*, vol. 13, no. 3, pp. 745, 2016.

[14] I. Idris, M. S. Robian, A. K. Mahamad, and S. Saon, "Arduino-based maximum power point tracking for photovoltaic systems," *ARPN J. Eng. Appl. Sci.*, vol. 11, no. 14, pp. 8805–8809, 2016.

[15] R. I. Putri, S. Wibowo, and M. Rifa'i, "Maximum Power Point Tracking for Photovoltaic Using Incremental Conductance Method," *Energy Procedia*, vol. 68, pp. 22-30, 2015,

[16] N. Femia, G. Petrone, G. Spagnuolo, and M. Vitelli, "Optimization of perturb and observe maximum power point tracking method," IEEE Trans. Power Electron., vol. 20, no. 4, pp. 963–973, 2005, doi: 10.1109/TPEL.2005.850975.

[17] Vu, T.-K., & Seong, S.-J. (2010). Comparison of PI and PR Controller Based Current Control Schemes for Single-Phase Grid-Connected PV Inverter. *Journal of the Korea Academia-Industrial Cooperation Society*, 11(8), 2968–2974. https://doi.org/10.5762/kais.2010.11.8.2968

[18] J. W. Umland and M. Safiuddin, "Magnitude and symmetric optimum criterion for the design of linear control systems: What is it and how does it compare with the others?" *IEEE Transactions on Industry Applications*, vol. 26, no. 3, pp. 489–497, Jun. 1990, doi: 10.1109/28.55962.

[19] P. Rajesh, R. I. Vais, S. Yadav, and P. Swarup, "A modified PI control for grid-tied inverters to improve grid injected current quality," *International Journal of Engineering and Technology (IJET)*, vol. 9, no. 3S, pp. 529–534, Jul. 2017, doi: 10.21817/ijet/2017/v9i3/170903S080.

[20] S. Dasgupta, S. N. Mohan, S. K. Sahoo, and S. K. Panda, "Application of four-switch-based three-phase grid-connected inverter to connect renewable energy source to a generalized unbalanced microgrid system," *IEEE Transactions on Industrial Electronics*, vol. 60, no. 3, pp. 1204–1215, Mar. 2013, doi: 10.1109/TIE.2012.2188258.

[21] E. Solas, G. Abad, J. A. Barrena, S. Aurtenetxea, A. Cárcar, and L. Zając, "Modular multilevel converter with different submodule concepts—Part I: Capacitor voltage balancing method," *IEEE Transactions on Industrial Electronics*, vol. 60, no. 10, pp. 4525–4535, Oct. 2013, doi: 10.1109/TIE.2012.2236651.

[22] R. Li, J. E. Fletcher, L. Xu, D. Holliday, and B. W. Williams, "A hybrid modular multilevel converter with novel three-level cells for DC fault blocking capability," *IEEE Transactions on Power Delivery*, vol. 30, no. 4, pp. 2017–2026, Aug. 2015, doi: 10.1109/TPWRD.2014.2364258.

[23] M. H. Mondol, M. A. Rahman, S. P. Biswas, M. R. Islam, M. F. Kibria, and K. M. Muttaqi, "A new integrated multilevel inverter topology for renewable energy transformation," *IEEE Transactions on Industry Applications*, vol. 59, no. 3, pp. 3031–3043, May-Jun. 2023, doi: 10.1109/TIA.2023.3264647.

[24] S. Shakeera and K. Rachananjali, "An innovative 11-level multilevel inverter topology with rotating trapezoidal SPWM for industrial and renewable applications," *Scientific Reports*, vol. 14, no. 1, 2024, doi: 10.1038/s41598-024-73791-0.

[25] B. Gopinath et al., "Renewable energy resource integrated multilevel inverter using evolutionary algorithms," *Automatika*, vol. 65, no. 3, pp. 1061–1078, 2024, doi: 10.1080/00051144.2024.2329494.

[26] A. Salem, H. Van Khang, K. G. Robbersmyr, M. Norambuena, and J. Rodriguez, "Novel three-phase multilevel inverter with reduced components for low- and high-voltage applications," *IEEE Transactions on Industrial Electronics*, vol. 68, no. 7, pp. 5978–5989, Jul. 2021, doi: 10.1109/TIE.2020.3001912.

[27] Wikipedia contributors, "Enel Green Power," *Wikipedia, The Free Encyclopedia*, 13 Mar. 2025. [Online]. Available: https://en.wikipedia.org/wiki/Enel_Green_Power.

[28] Wikipedia contributors, "Vikram Solar," *Wikipedia, The Free Encyclopedia*, 13 Mar. 2025. [Online]. Available: https://en.wikipedia.org/wiki/Vikram_Solar.

[29] Wikipedia contributors, "Smart grid in China," *Wikipedia, The Free Encyclopedia*, 13 Mar. 2025. [Online]. Available: https://en.wikipedia.org/wiki/Smart_grid_in_China.

[30] Wikipedia contributors, "Nuwakot Solar Power Station," *Wikipedia, The Free Encyclopedia*, 13 Mar. 2025. [Online]. Available:

https://en.wikipedia.org/wiki/Nuwakot_Solar_Power_Station.

[31] Wikipedia contributors, “Butwal Solar PV Project,” *Wikipedia, The Free Encyclopedia*, 13 Mar. 2025. [Online]. Available: https://en.wikipedia.org/wiki/Butwal_Solar_PV_Project.

[32] A. Kshatri, S. Dhami, and A. Bhatta, "Power Quality Enhancement Strategy In Grid Connected Dual Voltage Source Inverters Supplying Various Loads," *OODBODHAN*, vol. 7, no. 1, pp. 23–30, Dec. 2024, doi: 10.3126/oodbodhan.v7i1.75761.

[33] M. Nyaupane, S. Adhikari, G. Gupta, and S. Tiwari, “Comparison and analysis of maximum power point tracking algorithms for photovoltaic systems using genetic algorithm,” *2024 IEEE International Conference on Power System Technology (PowerCon)*, Kathmandu, Nepal, 2024, pp. 1–5.

[34] H. Slimane, J.-P. Gaubert, and F. Krim, “Real-time genetic algorithms-based MPPT: Study and comparison (theoretical and experimental) with conventional methods,” *Energy*, vol. 11, no. 16, p. 459, Feb. 2018, doi: 10.3390/en11020459.

[35] J. S. Goud et al., “Maximum power point tracking technique using artificial bee colony algorithm and hill climbing for PV array under partial shading conditions,” *IET Renewable Power Generation*, vol. 12, no. 16, pp. 1915–1922, 2018, doi: 10.1049/iet-rpg.2017.0902.

[36] R. Motamarri and B. Nagu, “GMPPT by using PSO based on Lévy flight for photovoltaic system under partial shading conditions,” *IET Renewable Power Generation*, vol. 14, no. 5, pp. 1155–1163, 2020, doi: 10.1049/iet-rpg.2019.1256.

[37] M. Fathi and J. A. Parian, “Intelligent MPPT for photovoltaic panels using a novel fuzzy logic and artificial neural networks based on evolutionary algorithms,” *Energy Reports*, vol. 7, pp. 1338–1351, 2021, doi: 10.1016/j.egyr.2021.02.051.

[38] F. A. Al Turki and M. M. Al Shammari, “Predicting the output power of a photovoltaic module using artificial intelligence-based approaches,” *Technology and Economics of Smart Grids and Sustainable Energy*, vol. 6, no. 1, 2021, doi: 10.1007/s40866-021-00064-0.

[39] M. Waqas and M. Jamil, "Power Quality Improvement Using Nine-Level Cascaded H-Bridge Voltage Source Inverter for PV Applications," *2024 12th International Conference on Smart Grid (icSmartGrid)*, Setubal, Portugal, 2024, pp. 429-434, doi: 10.1109/icSmartGrid61824.2024.10578256.

[40] A. Pradhan and B. Panda, “A simplified design and modeling of boost converter for photovoltaic system,” *International Journal of Electrical and Computer Engineering (IJECE)*, vol. 8, no. 1, pp. 141–149, Feb. 2018, doi: 10.11591/ijece.v8i1.pp141-1

# Appendix A: Published Paper Link

M. Nyaupane, S. Adhikari, G. Gupta and S. Tiwari, "Comparison and Performance Enhancement of Maximum Power Point Tracking Technique for Photovoltaic Systems using Genetic Algorithm," *2024 IEEE International Conference on Power System Technology (PowerCon)*, Kathmandu, Nepal, 2024, pp. 1-5, doi: 10.1109/PowerCon60995.2024.10870561.

# Appendix B: Plagiarism Test Report

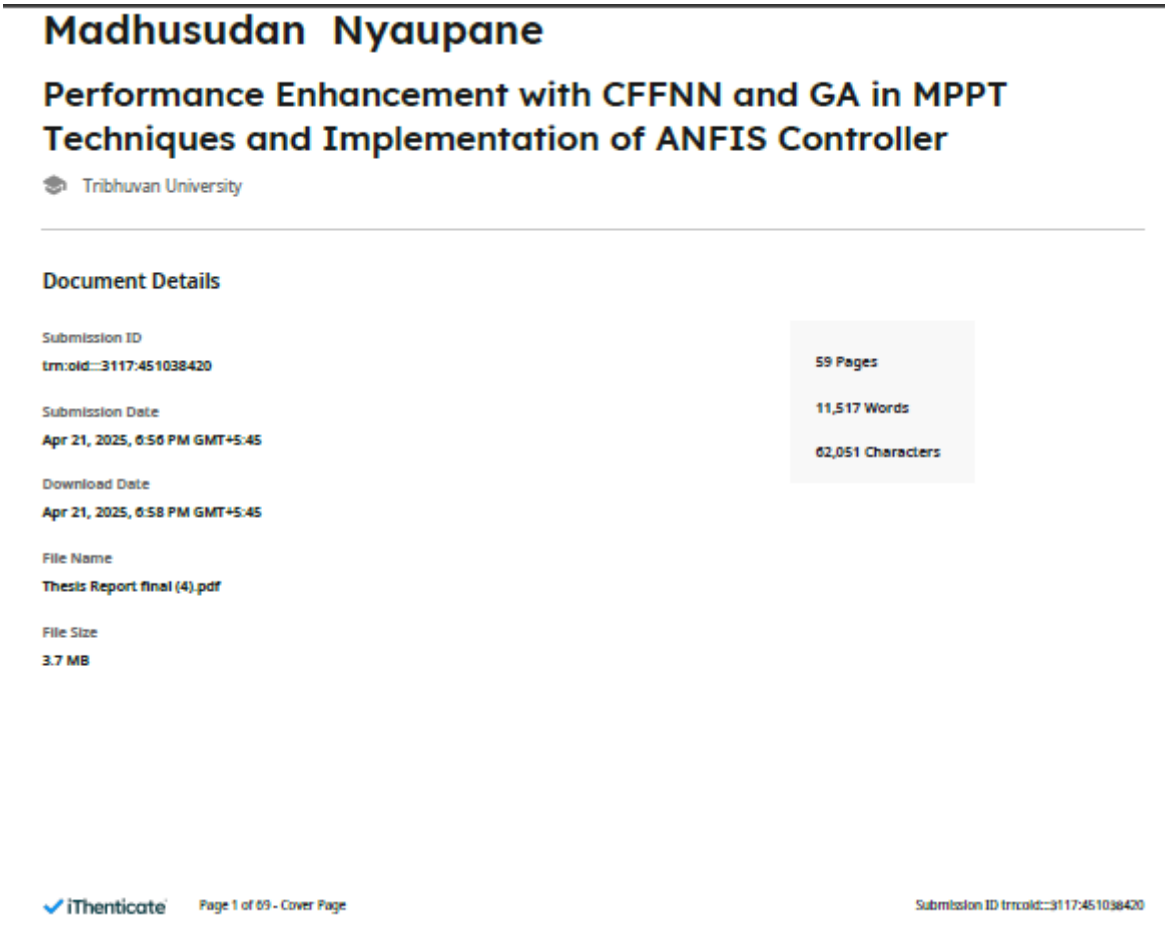

Madhusudan Nyaupane

Performance Enhancement with CFFNN and GA in MPPT Techniques and Implementation of ANFIS Controller

Tribhuvan University

Document Details

Submission ID
trn:oid:::3117:451038420

Submission Date
Apr 21, 2025, 6:56 PM GMT+5:45

Download Date
Apr 21, 2025, 6:58 PM GMT+5:45

File Name
Thesis Report final (4).pdf

File Size
3.7 MB

59 Pages

11,517 Words

62,051 Characters

iThenticate Page 1 of 69 - Cover Page Submission ID trn:oid:::3117:451038420

# 15% Overall Similarity

The combined total of all matches, including overlapping sources, for each database.

## Filtered from the Report

- Bibliography

## Match Groups

**145** Not Cited or Quoted 14%
Matches with neither in-text citation nor quotation marks

**0** Missing Quotations 0%
Matches that are still very similar to source material

**9** Missing Citation 1%
Matches that have quotation marks, but no in-text citation

**1** Cited and Quoted 0%
Matches with in-text citation present, but no quotation marks

## Top Sources

10% Internet sources
11% Publications
0% Submitted works (Student Papers)

## Integrity Flags

**1 Integrity Flag for Review**

**Replaced Characters**
10 suspect characters on 7 pages
Letters are swapped with similar characters from another alphabet.

Our system's algorithms look deeply at a document for any inconsistencies that would set it apart from a normal submission. If we notice something strange, we flag it for you to review.

A Flag is not necessarily an indicator of a problem. However, we'd recommend you focus your attention there for further review.

## Match Groups

- 145 Not Cited or Quoted 14%
  Matches with neither in-text citation nor quotation marks
- 0 Missing Quotations 0%
  Matches that are still very similar to source material
- 9 Missing Citation 1%
  Matches that have quotation marks, but no in-text citation
- 1 Cited and Quoted 0%
  Matches with in-text citation present, but no quotation marks

## Top Sources

10% Internet sources
11% Publications
0% Submitted works (Student Papers)

## Top Sources

The sources with the highest number of matches within the submission. Overlapping sources will not be displayed.

| | | |
|---|---|---|
| 1 | Internet | |
| 123dok.net | | <1% |
| 2 | Internet | |
| www.mdpi.com | | <1% |
| 3 | Publication | |
| Deepak Kumar Singh, Saibal Manna, A.K. Akella. "Grid Connected PV System Usin... | | <1% |
| 4 | Internet | |
| research.library.mun.ca | | <1% |
| 5 | Internet | |
| www.researchgate.net | | <1% |
| 6 | Internet | |
| livrepository.liverpool.ac.uk | | <1% |
| 7 | Internet | |
| koreascience.or.kr | | <1% |
| 8 | Internet | |
| link.springer.com | | <1% |

10 Internet

dergipark.org.tr <1%





11 Internet

scienceofbiogenetics.com <1%

12 Internet

journals.plos.org <1%

13 Internet

silo.pub <1%